A modeling study of shelf circulation off northern California in the region of the Coastal Ocean Dynamics Experiment: Response to relaxation of upwelling winds

Jianping Gan and J. S. Allen

College of Oceanic and Atmospheric Sciences, Oregon State University, Corvallis, Oregon, USA

Received 13 December 2000; revised 29 November 2001; accepted 11 December 2001; published 17 September 2002.

[1] A two-part modeling study of the wind-forced flow on the continental shelf off northern California in the region (37°–40°N) of the Coastal Ocean Dynamics Experiment (CODE) is pursued. This paper involves a process-oriented study with idealized wind stress forcing. *Gan and Allen* [2002] involves forcing with observed winds and heat flux for April–May 1982 and comparison of model results with CODE observations. A characteristic, but previously unexplained, response observed during CODE following the weakening, or relaxation, of southward upwelling favorable winds is the time-dependent development of northward currents over the inner shelf next to the coast. The presence of northward winds is not necessary for this occurrence. The objective in this paper is to investigate the dynamics of the shelf flow response to upwelling wind relaxation events under idealized conditions. In the basic case experiment a spatially uniform upwelling favorable southward wind stress of 0.1 Pa is applied to the ocean initially at rest. The stress is held constant for 10 days and then decreased linearly to zero over 3 days. In response to the southward wind stress, southward alongshore currents develop on the shelf accompanied by upwelling of cold, dense water near the coast. Considerable spatial variability in the shelf flow, clearly related to the alongshore variations in coastline and bottom topography, is found. The alongshore currents tend to separate from the coast south of capes, and the coldest surface water is found at those locations. As the winds decrease, northward currents, similar to those observed, develop on the inner shelf next to the coast at many alongshore locations. Examination of the alongshore momentum balances shows that the northward currents are forced by a northward pressure gradient force associated with negative alongshore pressure gradients. These pressure gradients are set up by the interaction of the wind-forced flow with the alongshore variations in shelf topography. In general, negative alongshore pressure gradients, intensified off Pt. Reyes and Pt. Arena by the gradient wind balance, are found south of capes. The negative pressure gradients geostrophically balance onshore flow at depth, and upwelling is strengthened in these locations. North of capes, positive pressure gradients that are primarily in balance with nonlinear advective effects are found. After the winds cease the forced across-shelf circulation weakens, and the resulting unbalanced negative pressure gradients south of the capes accelerate the alongshore currents northward. Processes with similar dynamics are found embedded in the more complex coastal ocean response to observed time varying winds by *Gan and Allen* [2002]. *INDEX TERMS:* 4219 Oceanography: General: Continental shelf processes; 4255 Oceanography: General: Numerical modeling; 4512 Oceanography: Physical: Currents; *KEYWORDS:* upwelling, relaxation, numerical modeling, shelf circulation

Citation Gan, J., and J. S. Allen, A modeling study of shelf circulation off northern California in the region of the Coastal Ocean Dynamics Experiment: Response to relaxation of upwelling winds, *J. Geophys. Res.*, *107*(C9), 3123, doi:10.1029/2000JC000768, 2002.

1. Introduction

[2] We conduct a modeling study of the wind-forced flow on the continental shelf off northern California in the region of the Coastal Ocean Dynamics Experiment (CODE). That region is north of San Francisco and is centered between Pt. Reyes (38°N) and Pt. Arena (39°N). The intensive field measurements in CODE took place in April–July 1981 and in April–July 1982 [e.g., *Beardsley and Lentz*, 1987]. During that time of year the winds are strong and predominately southward (upwelling favorable). We choose the region and time of the CODE field experiments for the model applica-

0148-0227/02/2000JC000768$09.00

tions to study interesting and unexplained features of the observed shelf flow fields and to enable direct model comparisons with the extensive CODE data set.

[3] This investigation is in two parts. In both parts we apply the Princeton Ocean Model (POM) [*Blumberg and Mellor*, 1987] for the hydrostatic primitive equations to a study of three-dimensional shelf circulation in a limited-area domain about 400 km in alongshore extent, with realistic coastline variations and shelf/slope bottom topography and with high grid resolution. The first part, presented here, involves a process-oriented study with idealized wind stress forcing. The purpose is to investigate and determine the dominant dynamical processes involved in the observed coastal ocean response to upwelling wind relaxation events [*Send et al.*, 1987; *Winant et al.*, 1987; *Huyer and Kosro*, 1987; *Kosro*, 1987]. The second part [*Gan and Allen*, 2002] involves simulations of the shelf flow field during April and May 1982 by forcing the model with observed winds and heat flux. This allows direct comparisons of model results with CODE current and temperature measurements.

[4] A map of the region of the CODE field experiment that shows the locations of the current meter moorings and of the atmospheric measurement stations during 1982 appears in Figure 1. We will utilize current measurements from moorings on the 1982 experiment N, C, and R lines. The predominantly southward winds during the CODE experiments exhibit fluctuations on typical synoptic timescales of several days. Strong southward winds are interrupted by brief periods of weak southward, or occasionally weak northward, winds. During these periods, termed upwelling wind relaxation events, the shelf flow field exhibits a characteristic response that includes the development of northward currents near the coast. Particularly evident from satellite images [*Send et al.*, 1987] are the effects of currents that flow northward around Pt. Reyes advecting warmer surface water northward near the coast.

[5] The coastal ocean response is illustrated for one relaxation event by the wind, current, and temperature measurements from CODE for April 1982 shown in Figure 2. Strong southward wind stress decreases from about 0.2 Pa to near zero values over a three day period beginning about 18 April. Following the decrease in southward wind stress, the alongshore currents at the R2, C2, and N2 moorings in water of about 60 m depth change direction from southward to northward. The measurements show that the deepest currents reverse direction first followed in order by the currents at decreasing depths. They also show that the reversal occurs first at C2 and a fraction of a day later at R2 and N2. The temperature measurements show that the temperatures increase in a corresponding manner with a delay of about 3 days. Note that the local alongshore component of the wind stress from buoy B13 decreased from strong southward, but did not become northward.

[6] The development of northward currents in response to relaxations of southward winds, illustrated for one event in Figure 2, is, in fact, a robust characteristic of the behavior of the shelf flow in the CODE region. During April–July 1982, five upwelling wind relaxation events with a qualitatively similar coastal ocean response were observed [*Send et al.*, 1987]. The presence of northward winds was not necessary for the development of northward currents. In spite of the regular occurrences of this coastal ocean

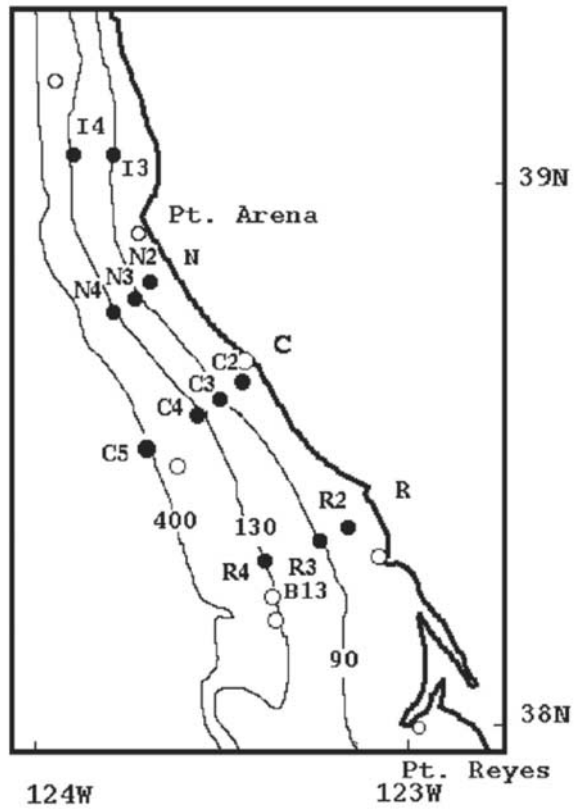

Figure 1. Map of the CODE region showing the topography and the locations of the current meter moorings (solid circles) in 1982. Stations where meteorological measurements were obtained are shown as open circles [adapted from *Limeburner*, 1985].

response to wind relaxations, a complete dynamical rationalization has not been established. In particular, solidly based explanations for the nature and origin of the force that drives the current northward have not been provided.

[7] In the direct model simulations forced by observed winds [*Gan and Allen*, 2002] we find a northward current response to wind relaxation events very similar to those observed during CODE. Because of the extremely complicated nature of the coastal ocean response to observed time-varying wind stress and because of the robust, but unexplained, nature of the relaxation response, we elect to conduct an additional process study of this phenomena with simplified wind stress time variability. The results of that study are reported here. The objective is to clarify the dynamical processes that lead to the northward currents near the coast in the CODE region in response to upwelling wind relaxation events.

[8] An outline of the paper is as follows. The formulation of the model and specification of the basic case experiment are described in section 2. Characteristics of the shelf flow behavior in the basic case experiment are described in section 3 followed in section 4 by an analysis of the dynamics of the shelf flow response to wind relaxation. In section 5, the dynamical processes associated with the establishment of alongshore variations in pressure and upwelling are investigated. The results are summarized and

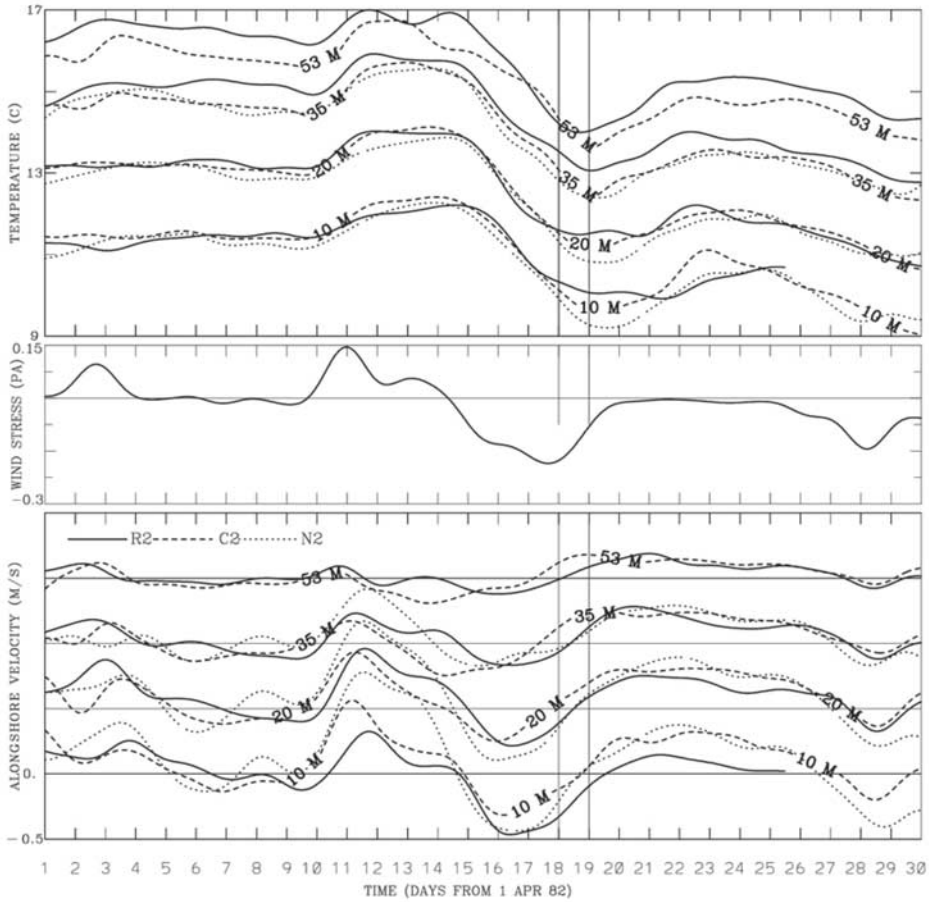

Figure 2. Time series of the alongshore component of the (middle) wind stress at buoy B13, (top) water temperature, and (bottom) alongshore velocity at depths of 10, 20, 35, and 52 m from the CODE moorings R2, C2, and N2. The time series have been filtered with a 36 hr low-pass filter. The alongshore direction for the wind stress and currents is 317°T. The temperatures and alongshore velocities at 20, 35, and 53 m depths are offset by 3°, 6°, and 9° C and 0.5, 1.0, and 1.5) m s^{-1}, respectively.

discussed in section 6. Appendix A contains a brief description of additional experiments and Appendix B contains a discussion of approximate potential vorticity dynamics.

2. Model Formulation

[9] The Princeton Ocean Model (POM) [*Blumberg and Mellor*, 1987] for the hydrostatic primitive equations with the *Mellor and Yamada* [1982] turbulence submodel embedded is applied to a high-resolution, limited area coastal domain that extends from about 36.6° to 40.5°N (Figure 3). Realistic coastline variations and shelf/slope topography are included from about 37° to 39.7°N. South of 37°N and north of 39.7°N, the across-shore topographic variations are uniform and equal to enable the use of periodic boundary conditions at the north and south boundaries. The model was successfully run in a similar size domain with open boundary conditions (J. Gan and J. S. Allen, On open boundary conditions for coastal circulation models, manuscript in preparation, 2002). with similar results, but the periodic channel was chosen purposefully here to avoid any questions of artificial alongshore pressure gradient setup by imperfect open boundary conditions.

[10] A curvilinear horizontal (x,y) grid is fit to the coastline, with straight axes utilized for the offshore and across-shore boundaries (Figure 3). The alongshore length of the straight offshore boundary (y axis), aligned along 335.5°T, is 469 km while the length of the across-shore boundaries (x axis) is 155 km. The numbers of grid cells in the (x,y) directions are (151, 359) which results in approximate grid sizes of $\Delta x \backsimeq 1$ km, and $\Delta y \backsimeq 1.3$ km. In the vertical, 60 sigma levels are utilized with grid spacing that varies so that there is higher resolution in the upper part of the water column. The shelf and slope bottom topography is a smoothed composite obtained from a variety of sources including ETOPO5 data (National Geodetic Center, Boulder, Colorado), Global Relief Data from the National Geophysical Center, and digitized data (1/240° from a high-resolution bathymetric map (National Oceanic and Atmospheric Administration (NOAA), NOS 1307N-18B, 1974). The maximum depth utilized is H_{max} = 2000 m. The Coriolis parameter $f = 0.9 \times 10^{-4}$ s^{-1} is constant.

[11] The velocity components in the (x,y) horizontal curvilinear coordinate directions are (u,v). The (x,y) coordinates are positive in the eastward and northward directions, respectively. The velocity component in the vertical z

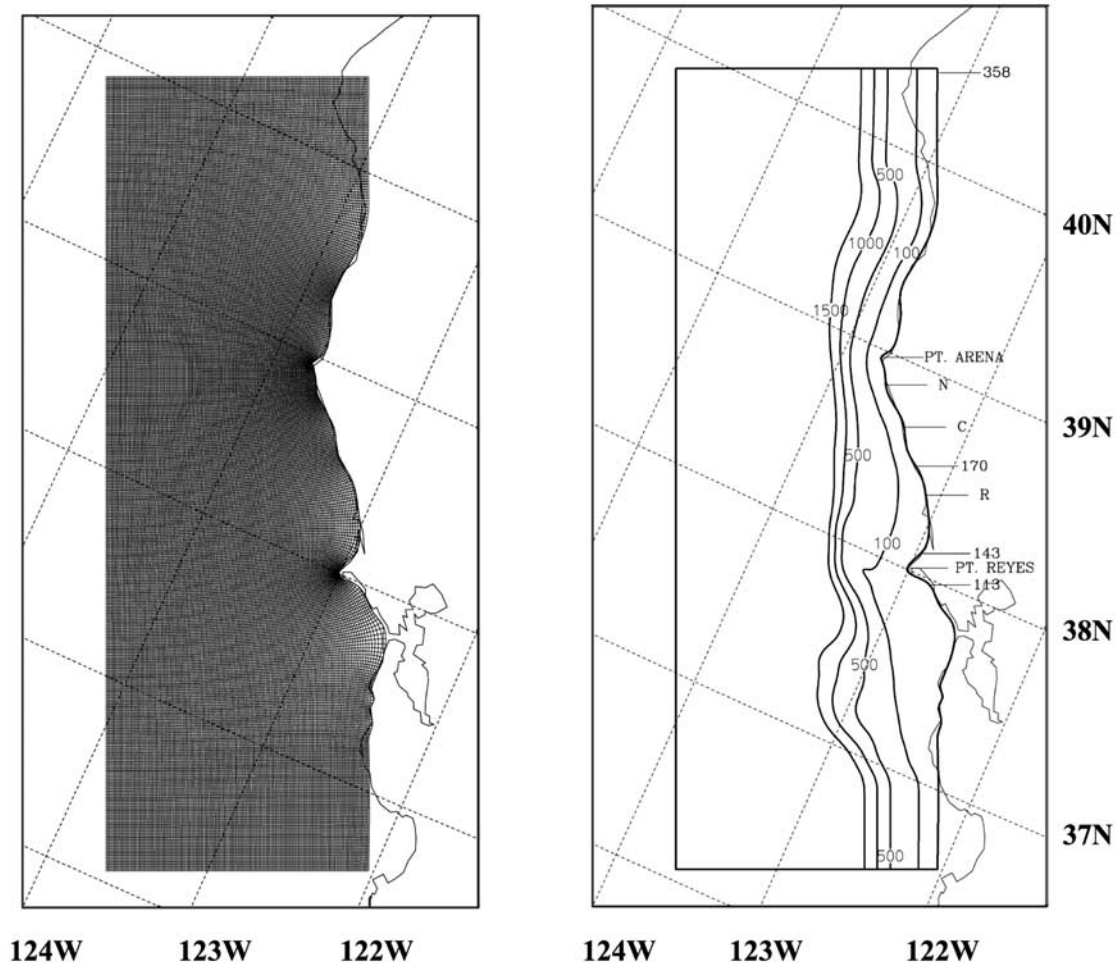

Figure 3. (left) Model curvilinear grid and (right) topography with the 100, 500, 1000, and 1500 m isobaths shown.

direction is w. We use the notation (U,V) for the depth-averaged velocities in the (x,y) directions. The surface elevation above the undisturbed free surface is η. The temperature, salinity and potential density variables are T, S, and σ_θ, respectively.

[12] Boundary conditions corresponding to periodic flow are utilized for all variables at the north and south boundaries. At the coastal boundary the water depth is approximately 10 m. The boundary conditions on the 10 m depth vertical sidewall at the coast are $u = 0$, $v_x = 0$ corresponding to a free slip condition on the tangential velocity component v, and $T_x = S_x = 0$. At the offshore boundary, the condition of zero normal depth-integrated velocity is applied, i.e., $U = 0$. In addition, we utilize $V_x = \eta_x = 0$ and *Orlanski* [1976] radiation conditions for the depth-dependent (u, v, T, S). The model is initialized with zero velocities and with horizontally uniform stratification. The initial temperature $T(z)$ and salinity $S(z)$ are obtained for this region from *Levitus and Gelfeld* [1992]. The resulting initial values of potential density $\sigma_\theta(z)$ and $N^2(z) = -(g/\rho_0)\sigma_{\theta z}$ are plotted in Figure 4.

[13] In the basic case experiment a spatially uniform, upwelling favorable, alongshore wind stress of 0.1 Pa is applied and held constant for 10 days. After 10 days, the wind stress is decreased linearly to zero over a period of 3 days and then maintained at zero after day 13. The alignment of the wind stress (317°T) is chosen to approximately match the major principal axis of the wind measured at Buoy B13 during the CODE experiment and is shown in Figure 5a. No surface heat flux is applied in the basic case experiment, but surface heat flux is applied in the simulation by *Gan and Allen* [2002]. Additional experiments to examine the sensitivity of the results to variations in form of the forcing are described in Appendix A.

[14] Other relevant parameter values utilized in POM for these experiments are the following. Horizontal diffusion processes are modeled with constant eddy coefficients with the values $A_M = A_H = 5\ \mathrm{m^2 s^{-1}}$. The bottom surface roughness $z_0 = 0.01$ m. The time step for the baroclinic mode is $\Delta t = 85$ s, while the time step for the barotropic mode is $\Delta t_{BT} = \Delta t/30$.

3. Characteristics of the Shelf Flow Response

[15] General characteristics of the shelf flow response in the basic case experiment may be seen in the plots of daily averaged surface velocity vectors, surface temperature, and surface elevation fields at days 6, 10, and 15 in Figures 5a–5c. The corresponding development of the alongshore velocity v and potential density σ_θ as a function of depth on an

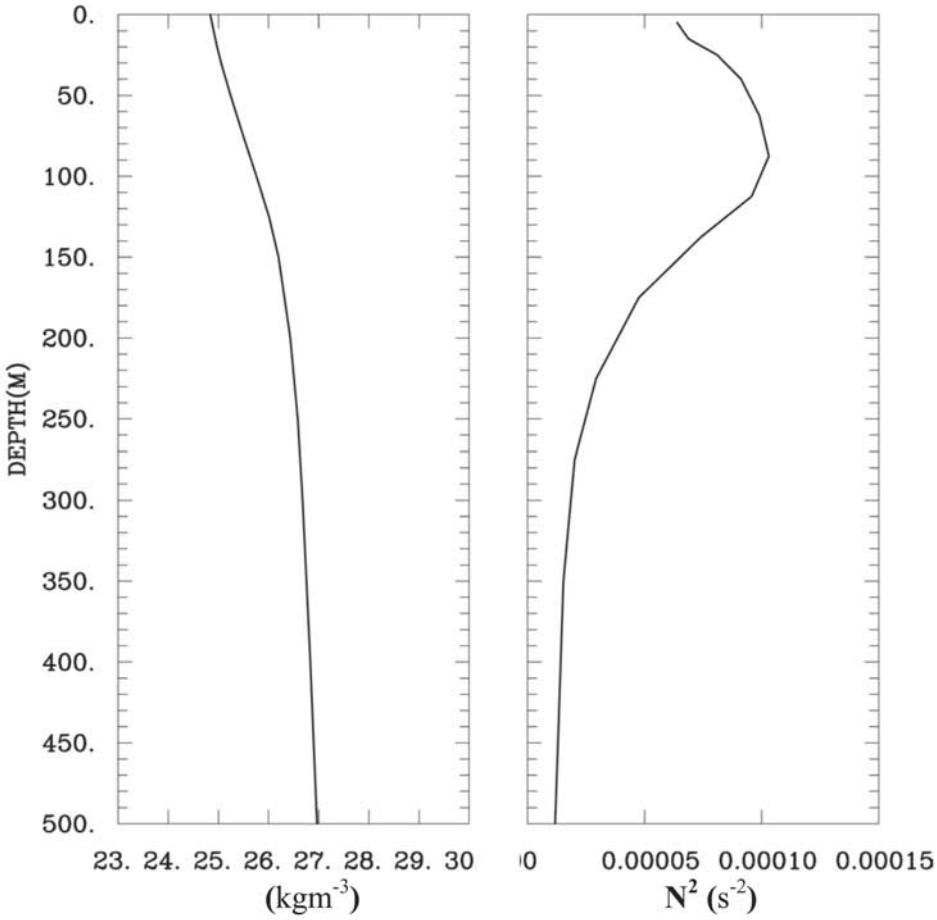

Figure 4. Initial values of σ_θ and N^2 as a function of depth.

across-shore section at the location of the CODE C line (Figures 1 and 2) is shown in Figure 6.

[16] The surface velocity vectors (Figure 5a) and the across-shore (x,z) section of v at C (Figure 6) show the presence on day 6, and strengthening by day 10, of an alongshore coastal jet over the shelf and upper slope. The corresponding surface temperature plots (Figure 5b) and the across-shore σ_θ sections at the C line (Figure 6) show the results of coastal upwelling evidenced by the presence of cold, dense water at the surface near the coast and the related upwelled isopycnals over the shelf and upper slope. These features are intensified on day 10.

[17] It is obvious that considerable variability exists in the shelf flow in the alongshore direction and that it is associated with variations in the coastline and in the shelf topography. A clear feature of the alongshore variability includes colder surface temperatures to the south of all capes. This occurs south of Pt. Reyes (38°N) and Pt. Arena (39°N) and also south of the smaller promontories at about 38.6°, 38.8°, and 39.3°N.

[18] An additional prominent feature of the alongshore variability is the separation of the alongshore coastal jet south of Pt. Reyes. By day 10, the largest surface currents associated with the coastal jet are displaced about 30 km offshore so that they are concentrated over the 100 m isobath. Weaker southward surface flow exists between this primary offshore deflected current and enhanced southward flow within 10 km of the coast.

[19] The surface elevation field η (Figure 5c) generally decreases toward the coast reflecting geostrophic balance with the surface velocities in the alongshore coastal jet. Alongshore variability is also evident in the elevation field. On days 6 and 10, the lowest elevations along the coast are found south of capes similar to the structure of the surface temperature field. In general, these variations lead to the presence near the coast of negative pressure gradients in the regions south of capes. The surface elevation field also clearly shows the offshore deflection of the coastal jet south of Pt. Reyes on day 10 and all along the coast south of Pt. Arena on day 15. Dynamical aspects of the topographically induced alongshore variability in the shelf flow field are discussed in more detail in section 5.

[20] The pattern of flow on day 15 after the southward winds have ceased is distinguished by the presence of northward surface velocities near the coast. These northward surface currents vary in strength along the coast, but are found at many locations from south of Pt. Reyes (38N) to north of Pt. Arena (39N). In particular, the region of northward surface currents with relatively large offshore extent of about 10 km around Pt. Reyes is evident in the day 15 surface velocity vectors. Also visible in the day 15 surface temperature field is the presence near the coast

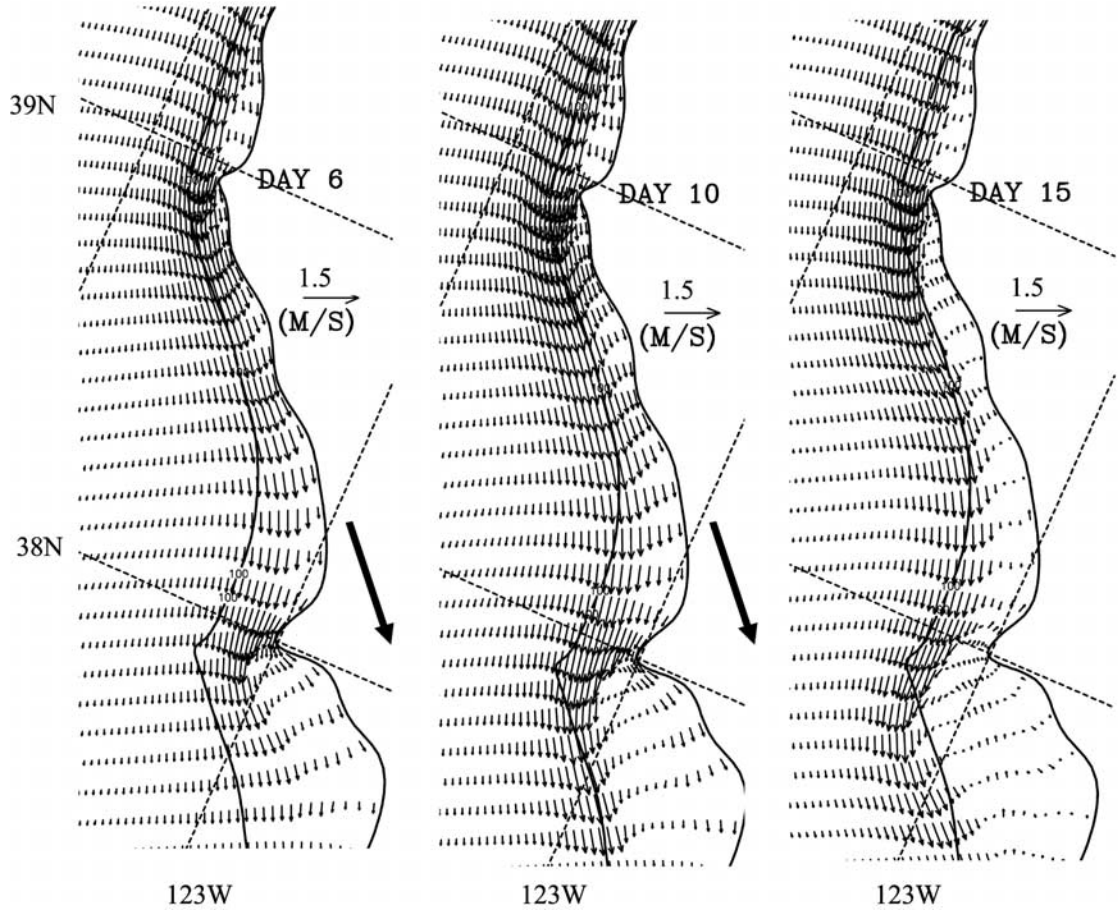

Figure 5a. Surface velocity vectors (m s^{-1}) on days 6, 10, and 15. The direction of the wind stress is indicated by the arrows on days 6 and 10. The 100 m isobath is shown.

north of Pt. Reyes of warmer surface water that evidently was advected northward around Pt. Reyes by the northward surface currents. The day 15 section of v at the C line (Figure 6) shows northward flow near the coast extending offshore in a wedge-shaped region of decreasing vertical extent such that at midshelf locations northward flow is found at depth underneath the inshore edge of the southward flowing coastal jet. By day 20 northward flow extends over much of the shelf. This reflects the strengthening in this particular region of a cyclonic eddy. The initial developments of this eddy may be seen in the day 15 surface elevation field (Figure 5c).

[21] Qualitative characteristics of the model response to the relaxation of upwelling favorable winds, as shown in Figures 5a–5c and 6 for day 15, are strikingly similar to those exhibited by the current and temperature measurements from the CODE experiment [*Send et al.*, 1987; *Winant et al.*, 1987; *Huyer and Kosro*, 1987; *Kosro*, 1987].

[22] Additional aspects of the alongshore and time variability of the shelf flow are shown in Figure 7 where across-shore sections of v are shown for days 10 and 15 at the locations of the N and R lines (Figure 3). For day 10, these sections, along with the C line section of v in Figure 6, show that the coastal jet width increases and the maximum surface velocity occurs farther from the coast as the shelf width increases from the N line south to the R line. For day 15, the sections all show northward, or weakened southward, currents near the coast with variations in strength depending on location. The change from day 10 to day 15 of the alongshore current structure is shown in Figure 8 by plots of the difference Δv between v on day 15 and v on day 10. The horizontal structure of Δv shows a northward flow change that is concentrated inshore adjacent to the coast. Additionally, the vertical structure of Δv at the R and C lines shows a tendency toward depth independence away from the bottom boundary layer.

[23] It is informative to look at the variations with time of the alongshore structure near the coast of the surface alongshore velocity v, the surface temperature T and the surface elevation η. These variables are plotted as a function of y at a location approximately 2.5 km from the coast for days 1–10 in Figure 9a and for days 11–19 in Figure 9b. The plots of T show considerable alongshore variability, starting as early as day 3, with colder water found initially at locations south of capes consistent with the day 6 surface T field in Figures 5a–5c. Also, evident is the development by day 10 of substantially colder surface water between Pt. Reyes and Pt. Arena than found in the other parts of the domain. During days 1–10, the surface elevation, which as a result of periodicity in y, has zero net alongshore pressure gradient, exhibits substantial regions of negative alongshore pressure gradients η_y south of Pt. Reyes and between Pt. Reyes and Pt Arena. Compensating positive values of η_y occur primarily over relatively small regions immediately

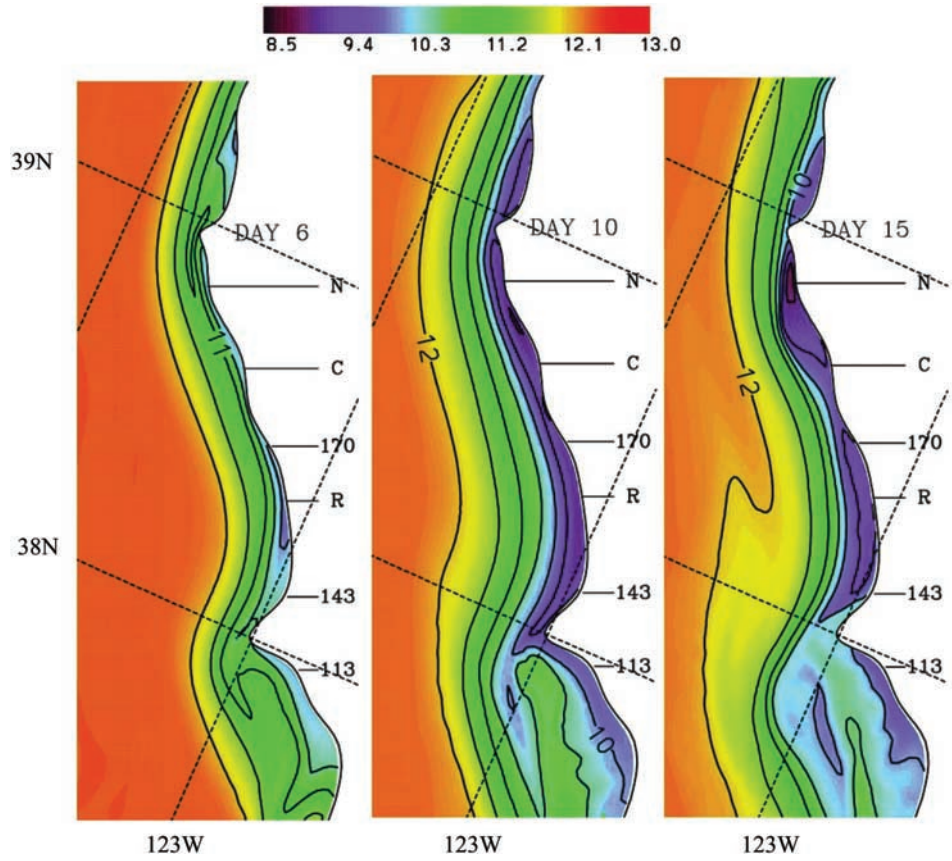

Figure 5b. Surface temperature (°C) on days 6, 10, and 15. The contour interval is 0.5°C.

north of Pt. Reyes and Pt. Arena. There is also a region of strong positive η_y about 60 km north of Pt. Arena. During days 1–10, the alongshore velocity v is negative corresponding to southward flow. For days 1–10 the dominant characteristics of the v behavior between about 100 km south of Pt. Reyes to 60 km north of Pt. Arena, are substantial spatial variations accompanied by time variations that generally decrease and change sign as time increases. This time variability is in contrast to the relatively steady increase in magnitude of v in the northern and southern regions of uniform topography. The time-dependent behavior and the resultant decreases in velocity magnitude between Pt. Reyes and Pt. Arena appear to be associated with the tendency in this region for the core of the alongshore coastal jet, which increases in strength with time, to move slowly offshore as time increases. That offshore movement and accompanying decrease in magnitude near the coast are evident in the day 6 to day 10 changes in the surface velocity vectors (Figure 5a) and in the alongshore velocity sections on the C line (Figure 6). In contrast, the core of the coastal jet in the northern and southern regions of uniform topography remains near the coast.

[24] For days 11–19 (Figure 9b), the variables v, T and η generally relax somewhat toward their initial values. The elevation η shows the development on day 13 of mostly negative gradients from south of Pt. Reyes to Pt. Arena. The most striking feature of the adjustment during these days is the eventual development of northward alongshore currents v over a major fraction of the entire domain. The dynamical processes associated with these adjustments will be discussed in section 4.

4. Dynamics of the Shelf Flow Response to Upwelling Wind Relaxation

4.1. Momentum Equations

[25] In this section we attempt to determine the dynamics of the processes involved in the shelf flow response to the upwelling wind relaxation in the basic case experiment. For that purpose, it is advantageous to examine the term balances in the momentum equations. We utilize the full z-dependent form of the alongshore y momentum equation,

$$H^{-1}\left\{\frac{\partial(vD)}{\partial t}+\left[\frac{\partial(uvD)}{\partial x}+\frac{\partial(v^2D)}{\partial y}+\frac{\partial(v\omega)}{\partial \sigma}\right]+fuD+\frac{D}{\rho_0}\frac{\partial p}{\partial y}-\frac{\partial}{\partial \sigma}\left(\frac{K_M}{D}\frac{\partial v}{\partial \sigma}\right)+F^{(y)}\right\}=0, \quad (1)$$

where we refer to the terms, in order from the left, by their usual descriptions: acceleration, nonlinear advection (including all the terms in square brackets), Coriolis force, pressure gradient, vertical diffusion, and horizontal diffusion. In this equation, in addition to the velocity variables

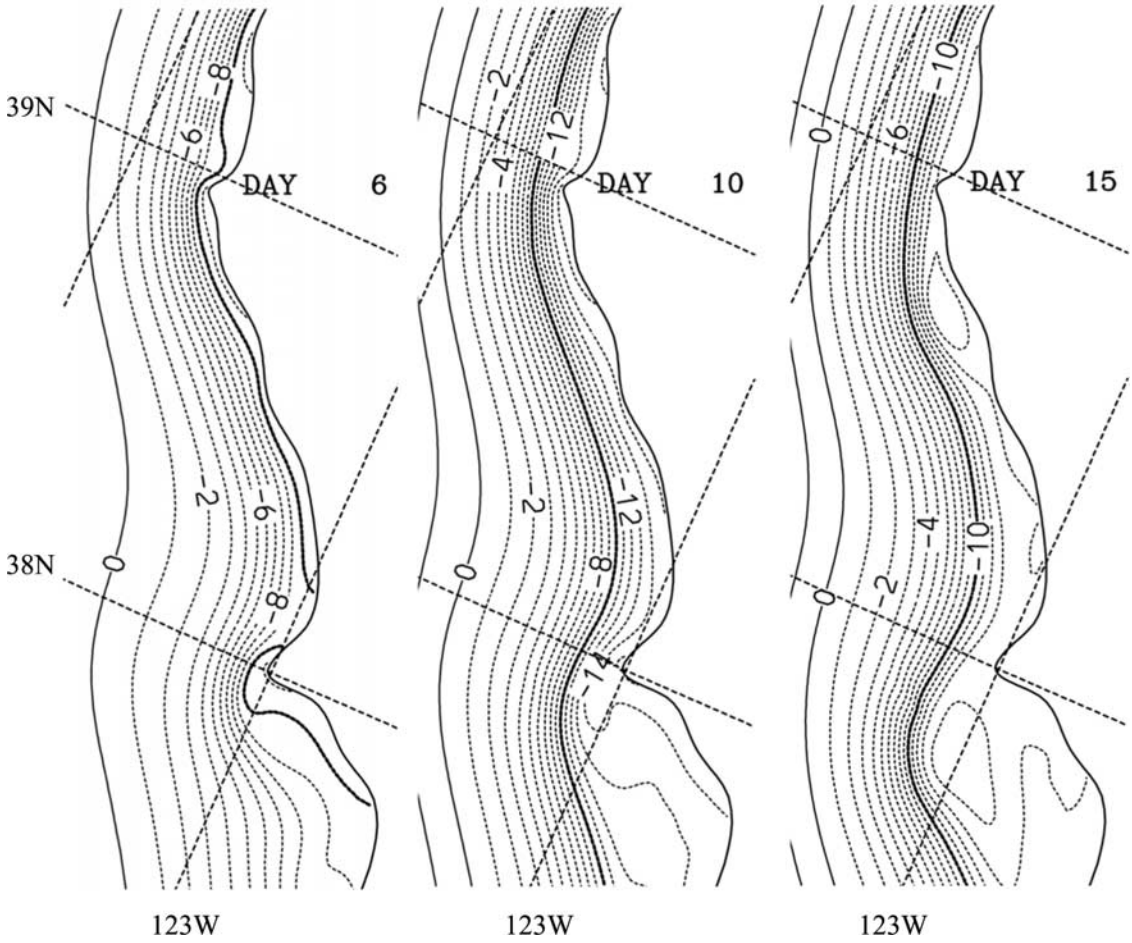

Figure 5c. Surface elevation (cm) on days 6, 10, and 15. The contour interval is 1 cm with a heavy contour line for −10 cm.

(u,v) in the (x,y) directions and the Coriolis parameter f defined previously, $D = \eta + H$ is the water depth, $H = H(x,y)$ is the undisturbed water depth, $\sigma = (z-\eta)/D$ is the sigma vertical coordinate, ω is a velocity normal to σ surfaces, p is pressure, ρ_0 is a constant reference density, K_M is the vertical kinematic viscosity and $F^{(y)}$ represents the horizontal diffusion terms [*Blumberg and Mellor*, 1987]. In terms of the surface elevation η and the density ρ, the pressure gradient term is

$$H^{-1}\frac{D}{\rho_0}\frac{\partial p}{\partial y} = H^{-1}\left\{gD\frac{\partial \eta}{\partial y} + \frac{gD}{\rho_0}\int_{\sigma}^{0}\left(D\frac{\partial \rho}{\partial y} - \sigma'\frac{\partial D}{\partial y}\frac{\partial \rho}{\partial \sigma'}\right)d\sigma'\right\}. \quad (2)$$

For calculations of the horizontal pressure gradient in equation (2) and in the x momentum equation, the initial density $\bar{\rho}(z)$ is first subtracted from total density ρ to reduce truncation errors. The numerical model equations are written in horizontal curvilinear coordinates. For simplicity in notation, we write the equations here in locally Cartesian form, but the variables are evaluated with respect to the curvilinear coordinates.

[26] We also find it useful to examine the behavior in the depth-averaged momentum equations, both in the across-shore x and alongshore y directions. We write those equations symbolically as

$$\frac{\partial U}{\partial t} + NLX - fV + \frac{1}{\rho_0}\frac{\partial P}{\partial x} - \frac{1}{\rho_0 D}\tau_S^{(x)} + \frac{1}{\rho_0 D}\tau_B^{(x)} = 0, \quad (3)$$

$$\frac{\partial V}{\partial t} + NLY + fU + \frac{1}{\rho_0}\frac{\partial P}{\partial y} - \frac{1}{\rho_0 D}\tau_S^{(y)} + \frac{1}{\rho_0 D}\tau_B^{(y)} = 0, \quad (4)$$

where $(\tau_S^{(x)}, \tau_S^{(y)})$ and $(\tau_B^{(x)}, \tau_B^{(y)})$ are the surface and bottom stress components, respectively, in the (x,y), directions, NLX and NLY represent nonlinear advection plus the horizontal diffusion terms, and the first, third, and fourth terms are the acceleration, Coriolis force, and pressure gradient terms, respectively.

4.2. Time Variation of Terms in the Depth-Integrated Alongshore Momentum Equation

[27] Time series of daily averaged terms in the depth-integrated alongshore momentum equation (4) from locations about 5.5 km offshore at the R line (water depth 55 m) and at the C line (water depth 58 m) are shown in Figure 10. Also shown are corresponding vector plots of the depth-

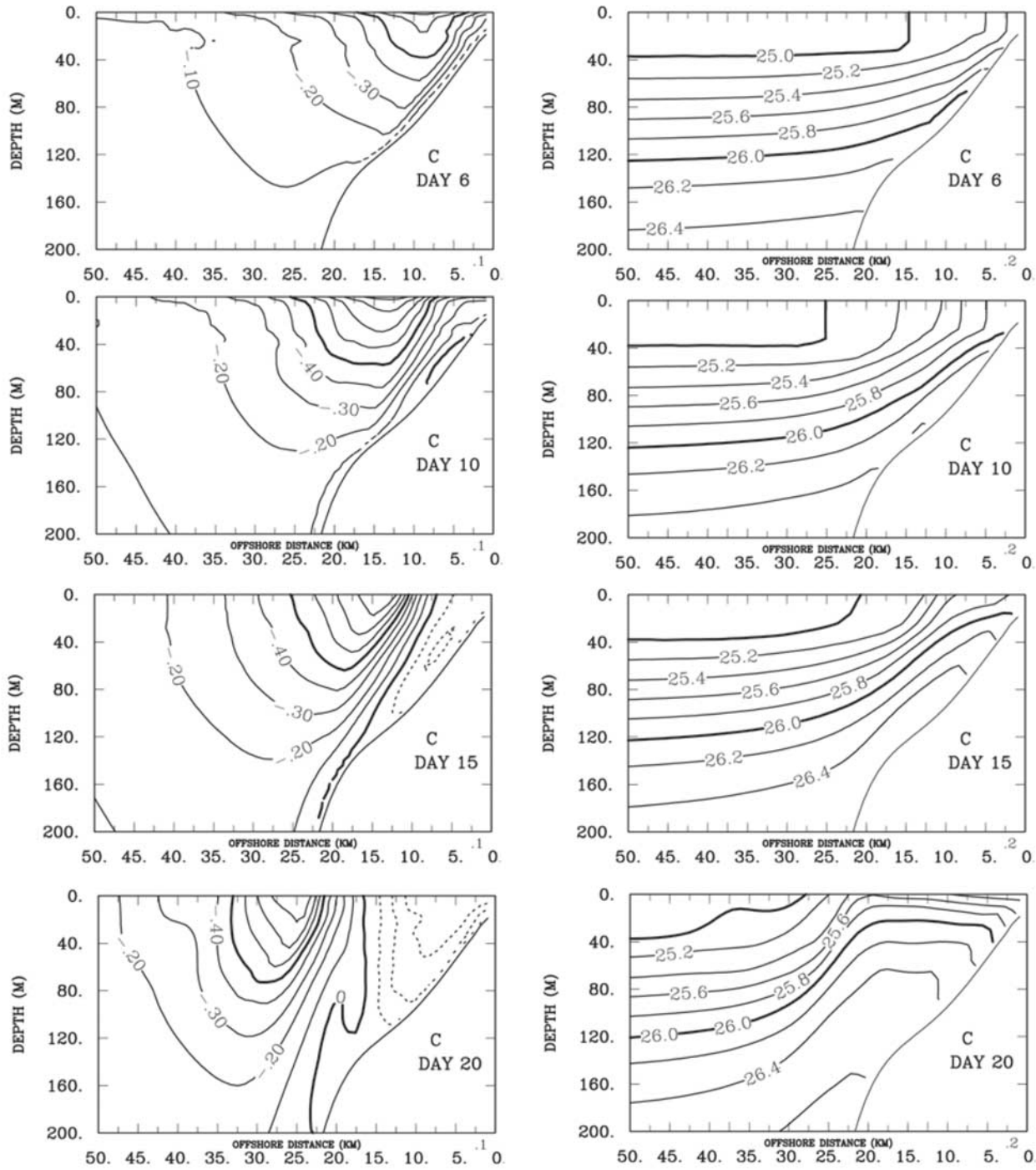

Figure 6. Across-shore sections of daily averaged alongshore velocity v (m s^{-1}) and potential density σ_θ (kg m^{-3}) at the location of the CODE C line on days 6, 10, 15, and 20. Negative (positive) values of v are indicated by solid (dashed) contours. The contour interval for velocity is 0.1 m s^{-1} with heavy contour lines for 0 and -0.5 m s^{-1}. The contour interval for σ_θ is 0.2 kg m^{-3} with heavy contour lines for 25 and 26 kg m^{-3}.

averaged velocity at the same locations. The surface wind stress term shows the time variability of the forcing. At both locations the velocity vector plots show southward currents that initially increase in magnitude from zero until about day 6, followed by a decrease in magnitude and eventual reversal of current direction to northward around day 13. The decrease in magnitude starting on day 6 corresponds to the movement offshore of the core of the coastal jet. The northward currents are those previously discussed and associated with the response to the relaxation of upwelling winds. In the

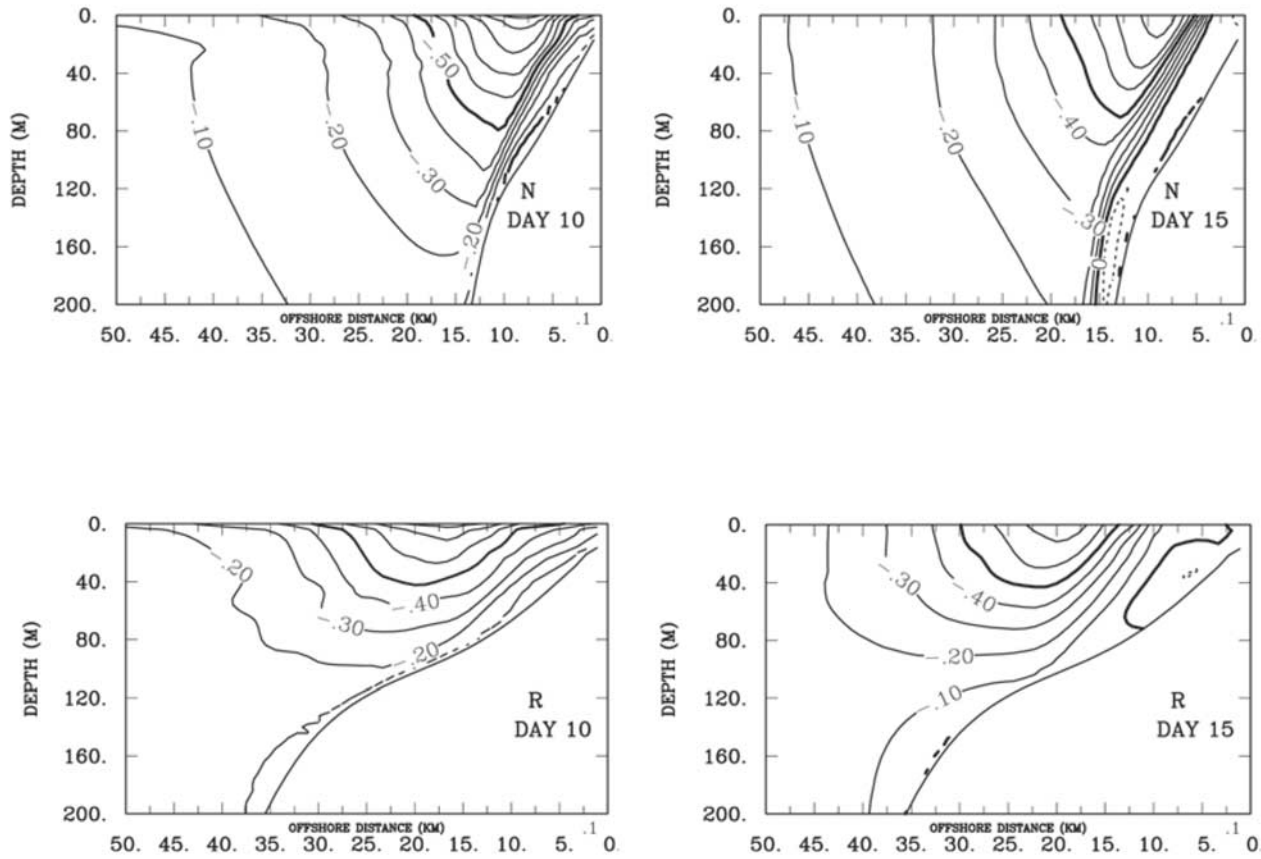

Figure 7. Across-shore sections of daily averaged alongshore velocity v (m s^{-1}) at the locations of the CODE N and R lines on days 10 and 15. Negative (positive) values of v are indicated by solid (dashed) contours. The contour interval is 0.1 m s^{-1} with heavy contour lines for 0 and -0.5 m s^{-1}.

term balances, the wind stress is balanced initially by the negative southward acceleration of this alongshore current. At the R line, the initially negative bottom stress term increases in magnitude, leveling off after 4 days, and makes an appreciable contribution, along with the depth-integrated Coriolis force, to balancing the wind stress. The pressure gradient term becomes negative after day 7 and helps balance the positive northward acceleration of the current between days 7 and 13. After the wind stress goes to zero on day 13, the pressure gradient is essentially the only negative term and is thus clearly responsible for the northward acceleration of the alongshore current during this period.

[28] At the C line, the initial response differs in that a negative pressure gradient develops immediately and grows in magnitude until about day 8. Part of the negative pressure gradient appears to be balanced by the Coriolis term. This presumably reflects a geostrophic balance of the effective alongshore current which, as seen from the velocity vectors, is directed onshore with respect to the local direction of the y coordinate. The bottom stress opposes the wind stress until about day 9 but is relatively small. Again, as at the R line, the negative pressure gradient appears to contribute support to the positive acceleration of the alongshore current after day 5 and is clearly the only term responsible for positive acceleration after the wind forcing ceases on day 13. Of note here is the increase after day 11 of the positive bottom stress term which opposes the northward current driven by the pressure gradient.

[29] It is evident from the term balances in Figure 10 that negative pressure gradients that give a northward pressure gradient force are the forcing mechanisms for the northward currents found near the coast following the wind relaxation. As will be shown in Section 5, the sea surface elevation gradients give an indication of the pressure gradients over the shelf through much of the water column. Thus, we get an appreciation of how the pressure gradients are set up from the plots at surface elevation fields on days 6 and 10 in Figure 5c. Both surface elevation and surface temperature fields are influenced strongly by shelf and coastline topography. Locations south of capes where the coldest water is found at the surface correspond closely to the locations of the lowest values of surface elevation. This we take as an indication that the alongshore variability in the coastal upwelling response and in the pressure field are closely linked dynamically.

5. Dynamics of Alongshore Variations in Pressure and Upwelling

[30] The most important immediate questions raised by the results in section 4 are how alongshore variations in the pressure field and in coastal upwelling are established in the

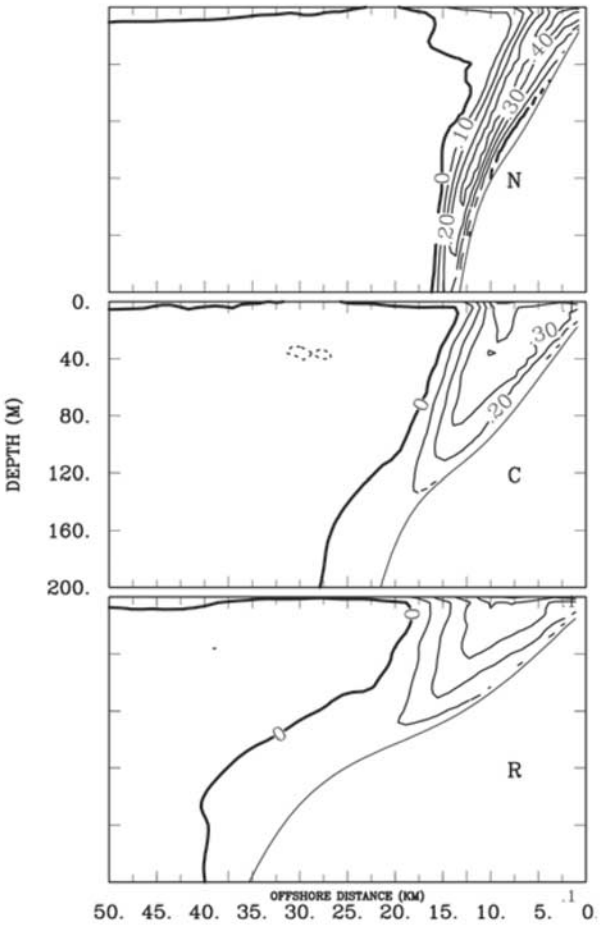

Figure 8. Across-shore sections of the daily averaged alongshore velocity difference Δv (v on day 15 minus v on day 10) at the N, C, and R lines. Negative (positive) values of Δv are indicated by solid (dashed) contours. The contour interval is 0.1 m s^{-1} with a heavy contour line for 0.

upwelling wind-forced shelf flow and how they depend on the shelf topography. It is clear that the presence of capes has a large influence on the behavior at the shelf flow. To examine more closely the flow variations associated with capes, we concentrate on the early time behavior in the region around Pt. Reyes.

5.1. Flow in the Vicinity of Pt. Reyes

[31] Daily averaged fields on day 3 of surface elevation and surface temperature (Figures 11a and 11b) show the development of low surface elevation and low surface temperatures south of Pt. Reyes. Also shown (Figure 11f) are contours of the depth-integrated alongshore pressure gradient term from (4) which illustrates, as anticipated from the elevation fields, the negative and positive pressure gradients south and north of Pt. Reyes, respectively. The velocity vectors (Figure 11d) show an increase in the magnitude of the surface currents directly offshore and to the south of Pt. Reyes, accompanied by an offshore deflection of the coastal jet south of the point. The velocity vectors at depth on the $\sigma = -0.658$ surface (Figure 11e) show a similar structure with reduced magnitudes in the coastal jet, but also clearly illustrate the presence of onshore flow south of the cape. The change of potential density $\Delta\sigma_\theta = \sigma_\theta - \sigma_\theta(t = 0)$, at the bottom (Figure 11c) shows the largest increase in $\Delta\sigma_\theta$ just south of Pt. Reyes, reflecting the advective effects of the onshore flow at depth seen in Figure 11e. Positive vertical velocities result from this onshore flow and lead to corresponding decreases in the surface temperatures (Figure 11b).

[32] The decrease in surface elevation south of Pt. Reyes appears to be related through geostrophic balance to the increase in magnitude of the alongshore coastal current as it flows around the point. A plot (Figure 12) of the surface elevation and the surface alongshore velocity v and of the terms in the across-shore depth-averaged momentum balance (equation (3)) as a function of alongshore coordinate y at a location approximately 5.5 km offshore on day 3 shows the increase in magnitude of v near the points and provides additional information about the alongshore variability. The primary across-shore momentum balance is between the Coriolis force and the pressure gradient, i.e., it is geostrophic as anticipated. In the vicinity of Pt. Reyes and Pt. Arena, however, the nonlinear advection terms make a substantial positive contribution to the balance of an increased negative pressure gradient. This situation evidently reflects a gradient wind-like balance [*Holton*, 1992], expressed approximately as

$$\frac{V^2}{R} - fV = -\frac{1}{\rho_0}\frac{\partial P}{\partial x}, \tag{5}$$

where R is the local radius of curvature of the streamlines. The nonlinear centrifugal force term V^2/R is evidently important because of the increased values of V^2 and decreased values of R near these points. This balance contributes to the local minima of the surface elevations found at essentially the same locations. These locally lowered elevations intensify the alongshore pressure gradients in the vicinity of Pt. Reyes and Pt. Arena.

[33] Additional information on the alongshore variability of the shelf flow and of the dynamical balances may be obtained from plots (Figure 13) of the potential density σ_θ and of the terms in the full z-dependent alongshore momentum equation (1) as a function of depth z and the alongshore coordinate y at a distance from the coast of approximately 2.5 km. In general, we see positive vertical diffusion in a surface layer of about 20 m depth that extends, with some variations in the strength, over the full domain. This reflects the near-surface frictional layer response to the southward wind stress as expected. A negative Coriolis force term, fu, reflecting offshore flow in the surface layer, tends to balance the vertical diffusion in an Ekman layer. There is, however, considerably more alongshore variability in strength of the Coriolis force term, as pressure gradient and nonlinear effects also contribute to balance the vertical diffusion at different locations. The offshore flow in the surface layer is accompanied by onshore flow, i.e., by a positive Coriolis force term fu, in a bottom layer which appears, from the apparent balance by negative vertical diffusion terms in many places, to be a bottom Ekman layer at those locations. This onshore flow at depth is clearly associated with the presence of increased values of σ_θ, both at depth and at the surface. Strong negative and positive pressure gradients

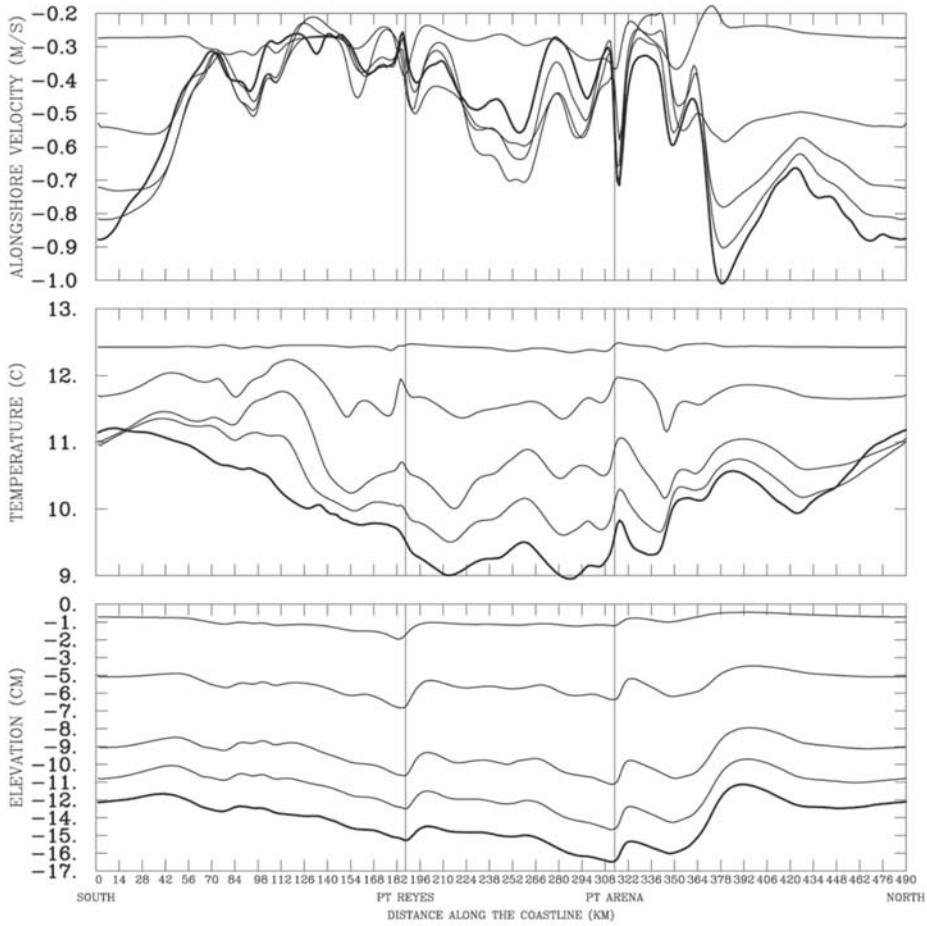

Figure 9a. Daily averaged values of surface alongshore velocity, surface temperature, and surface elevation as a function of distance y along the coast from locations approximately 2.5 km offshore for days 1, 3, 6, 8, and 10. In general, temperature and elevation decrease as time increases, as does alongshore velocity at $y = 0$. The values for day 10 are plotted with heavy lines.

south and north, respectively, of Pt. Reyes and Pt. Arena are evident as is the tendency for these gradients to be independent of depth. The latter feature allows the nature of the setup of horizontal pressure gradients to be deduced from the behavior of the sea surface elevation fields as mentioned previously.

[34] If we focus in Figure 13 on the region around Pt. Reyes, we see the depth and alongshore dependence of the processes discussed in connection with Figures 11 and 12. Strong onshore flow at depth (positive Coriolis force), balanced just south of Pt. Reyes by the negative pressure gradient and farther south by vertical diffusion in a frictional bottom boundary layer, is clearly associated with the increased values of σ_θ in this region. The offshore flow in the surface layer is stronger toward the south in the region of the bottom frictional balance. The positive pressure gradient north of Pt. Reyes is balanced partly by the Coriolis force, reflecting across-shelf veering of the primarily geostrophically balanced coastal jet, but also by a substantial contribution from the nonlinear advection terms. A similar positive pressure gradient and negative nonlinear advection balance is found north of Pt. Arena. Also similar to Pt. Reyes, the negative pressure gradient south of Pt. Arena balances onshore flow below the surface layer and vertical diffusion in the surface layer.

[35] To help understand the flow asymmetry north and south of Pt. Reyes, we plot in Figure 14 the velocity and density fields on across-shelf sections at locations 113 and 143 (Figure 5b) for days 3 and 6. We also plot in Figures 15 and 16 the terms in the alongshore momentum balance (equation (1)) and also the vertical velocity w on the same sections for the same days. At location 143, north of Pt. Reyes, we see the development on day 3, and strengthening by day 6, of the coastal jet. We also see the accompanying upwelling toward the coast of the isopycnals. At section 113 south of Pt. Reyes, we see the movement of the coastal jet offshore from day 3 to day 6. Also evident is the presence at the surface of water of density $\sigma_\theta > 25.0$ over a considerably larger across-shore extent at 113 than at 143 reflecting stronger upwelling at 113.

[36] In the momentum balance on day 3 (Figure 15), the presence of a positive diffusion term in a surface layer of

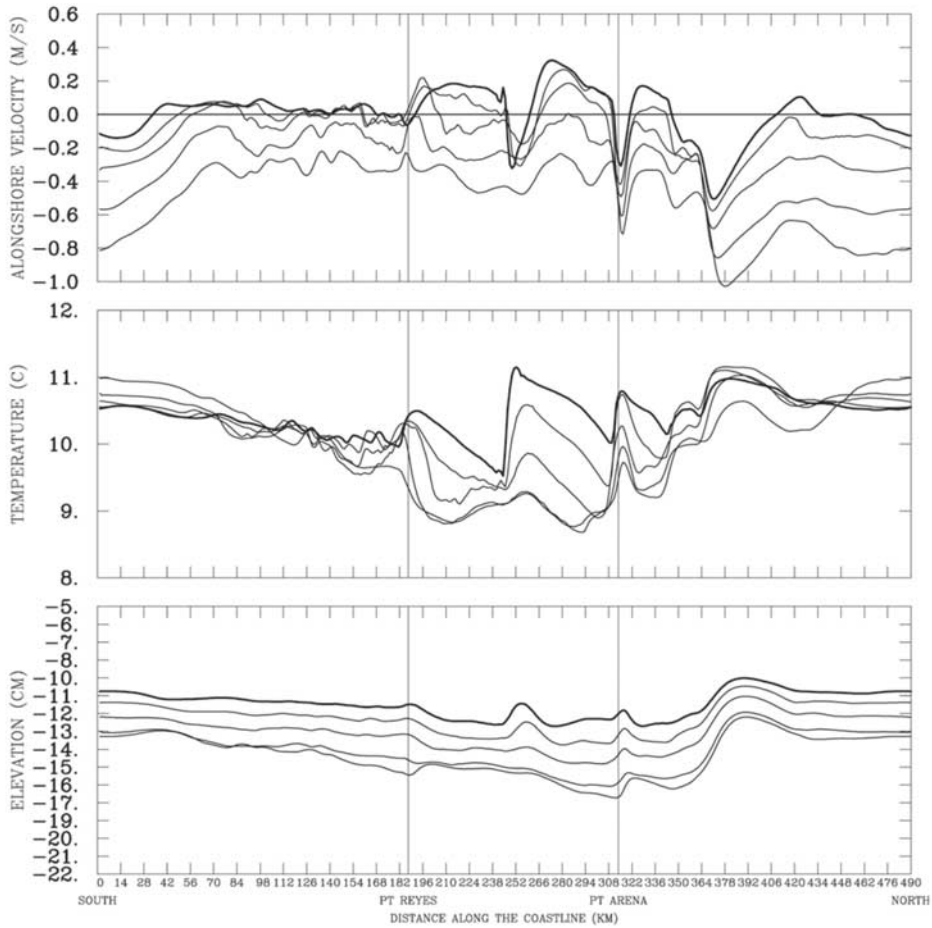

Figure 9b. Daily averaged values of surface alongshore velocity, surface temperature, and surface elevation as a function of distance y along the coast from locations approximately 2.5 km offshore for days 11, 13, 15, 17, and 19. In general, all variables increase as time increases. The values for day 19 are plotted with heavy lines.

thickness about 20 m, clearly balanced by a negative Coriolis term in an Ekman-like manner, is evident at distances from the coast greater than 25 km on both sections. A major difference in behavior between sections 113 and 143 is found in the pressure gradient and Coriolis force balance at depth over the shelf. At 113, a negative pressure gradient balances a positive Coriolis force term, corresponding to onshore flow, where at 143 a positive pressure gradient balances offshore flow. In addition, at 143 there is a negative contribution from nonlinear effects balancing the positive pressure gradient within about 5 km from the coast. Importantly, the onshore flows over the shelf at 113 is accompanied by relatively large vertical velocities w over an extensive part of the water column inshore of 20 km. In contrast, the vertical velocities at 143 are confined to a much smaller region in a thin bottom boundary layer. This difference in behavior, north and south of Pt. Reyes, of the onshore velocity and the resultant vertical velocity appears to be the major contributor to be the enhanced upwelling south of Pt. Reyes.

[37] The momentum balances on day 6 (Figure 16) at 143 show features similar to those found on day 3 at 143 except that the pressure gradient and Coriolis term balance is strengthened and extends farther offshore over the shelf. In addition, the negative nonlinear advective effects near the coast are also strengthened and are important in a larger region that extends offshore about 10 km. Negative advection terms are consistent with negative values of vv_y corresponding to the spatial acceleration of the coastal jet just north of Pt. Reyes as shown by the y variation of v in Figure 12. The vertical velocity w over the shelf remains primarily restricted to the bottom boundary layer.

[38] The momentum balances at 113 on day 6 show interesting differences from those on day 3 reflecting the complex time-dependent evolution of the flow south of Pt. Reyes. The acceleration term clearly exhibits positive values on the inshore side of the coastal jet (Figure 14) and negative values on the offshore side corresponding to the movement offshore of a strengthening coastal current. The negative values on the offshore side of the jet are balanced by nonlinear advective effects as might be anticipated from the behavior of the velocity fields shown in Figures 5a–5c and 11. The positive accelerations on the onshore side of the jet, on the other hand, are balanced by the negative pressure gradients. The vertical diffusion term shows positive values in a surface boundary layer that

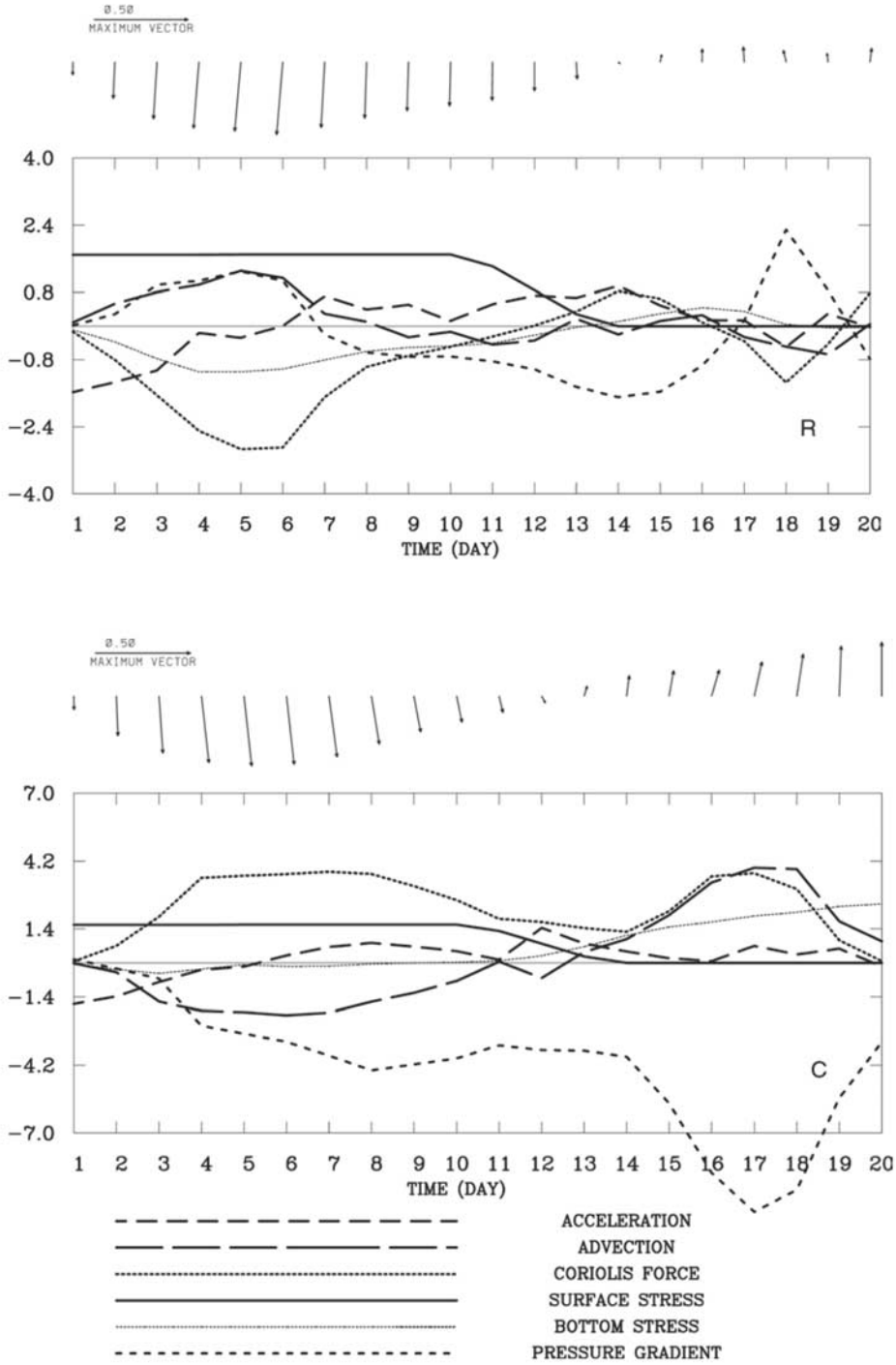

Figure 10. Time series of terms in the depth-averaged alongshore momentum equation (4) (in m s^{-2}, averaged over 24 hours, multiplied by 10^6) from locations about 5.5 km offshore at the R (water depth 55 m) and the C (water depth 58 m) lines. Time series of corresponding daily averaged depth-averaged velocity vectors from the same locations are also shown. The velocity vectors are plotted such that the vertical axis in the figure is aligned with the local y coordinate direction. The value of the daily average plotted, for example, at day 1, corresponds to a 24 hr average from $t = 0$ to $t = 1$ day.

extends to depths of about 30 m over the outer shelf. From the shelf break, at 35 km from the coast, inshore to about 20 km from the coast, a negative vertical diffusion term near the bottom indicates the presence of a bottom Ekman layer under the offshore-displaced coastal jet (Figure 14). A striking feature is the abrupt termination of this balance on the inshore side of the jet. Over the midshelf region, between about 15 and 30 km from the coast, a negative

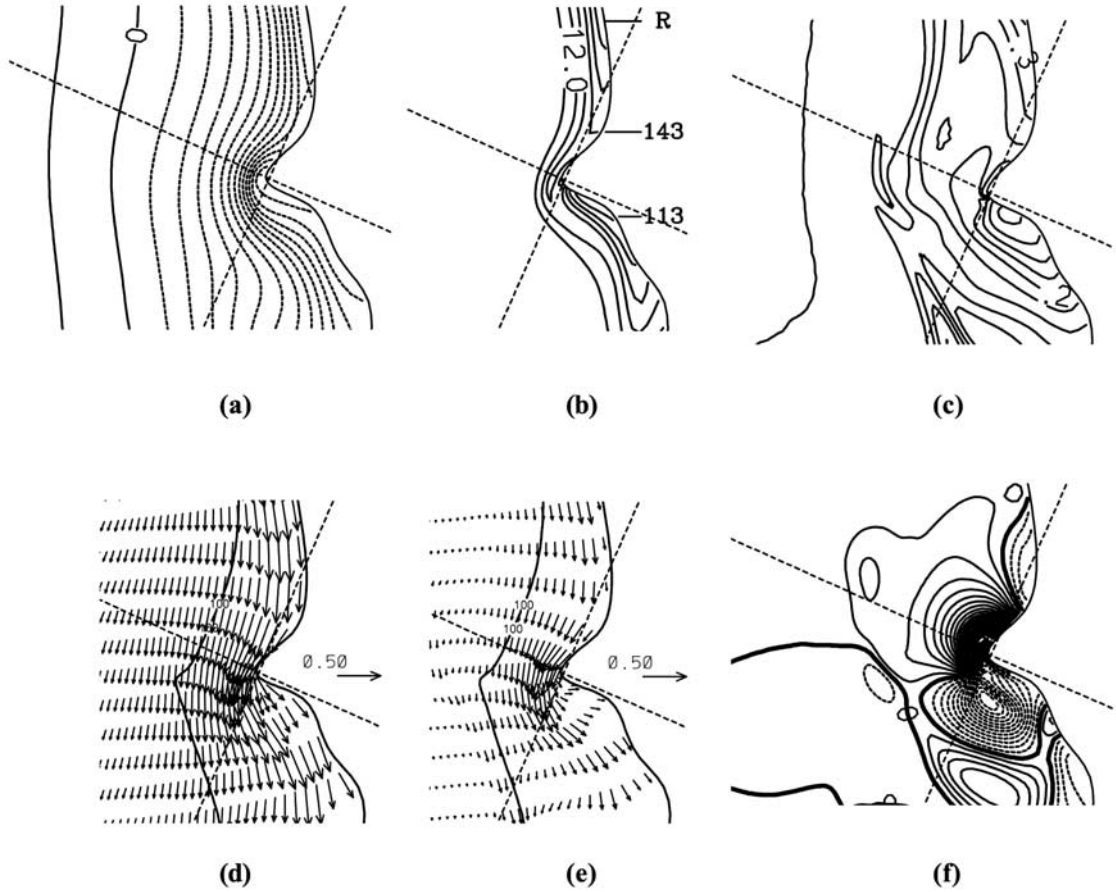

Figure 11. Daily averaged fields on day 3 of (a) surface elevation (interval 0.5 cm), (b) surface temperature (interval 0.2 C), (c) $\sigma_\theta - \sigma_\theta$ ($t = 0$) at the bottom (interval 0.05 kg m^{-3}), (d) surface velocity vectors (m s^{-1}), (e) velocity vectors (m s^{-1}) at $\sigma = -0.658$, and (f) depth-averaged y pressure gradient (multiplied by 10^6; interval 1 m s^{-2} with a heavy contour line for 0).

pressure gradient balances a positive Coriolis term. This positive onshore flow indicated by the Coriolis term again appears to be directly linked to strong vertical velocities w, which are found over the mid and outer shelf through much of the water column.

[39] On day 6 the strong vertical velocities on the mid and outer shelf at 113 are located on the inshore edge of the coastal jet and are clearly associated with the upwelled isopycnals at this location on the shelf (Figure 14). The region of large vertical velocities also coincides with that of relatively large acceleration and nonlinear advection effects in the alongshore momentum balance (Figure 16). These factors seem to indicate that this midshelf and outer-shelf upwelling is being strongly influenced by nonlinear potential vorticity dynamics associated with the separation of the coastal jet south of Pt. Reyes. To investigate that possibility further, we examine in Figure 17 terms in the approximate vorticity equation (B11) derived in Appendix B, on an across-shore section at 113 on days 3 and 6. The terms plotted are specified in equations (B12a), (B12b), and (B12c) and represent the time rate of change, nonlinear, and vertical diffusion terms. The sum of these three terms is also plotted as is fw_z. If the vorticity equation (B11) is a good approximation, the sum should equal fw_z.

[40] On both days 3 and 6 reasonable agreement between the sum and fw_z is evident. All terms have largest magnitudes in the regions over the shelf where the vertical velocity is largest (Figures 15 and 16). There is a tendency for the time rate of change to balance the nonlinear term, presumably reflecting nonlinear advective vorticity adjustment processes in the separated coastal jet. The vertical diffusion term is relatively large in the regions of the surface and bottom boundary layers where there are appreciable x gradients as indicated in Figures 15 and 16. Overall, all three terms, including a notably strong contribution from the nonlinear term, appear to balance fw_z and, hence, to help determine the horizontal location and vertical structure of the vertical velocity w. This suggests that the location and strength of the upwelling at 113 on days 3 and 6 is influenced by nonlinear dynamical processes associated with the separation of the coastal jet. Those separation processes are complex and obviously require additional investigation that is not attempted here.

5.2. Upwelling Between Pt. Reyes and Pt. Arena

[41] Between days 6 and 10, a dominant feature of the shelf flow response over the full domain is the continued

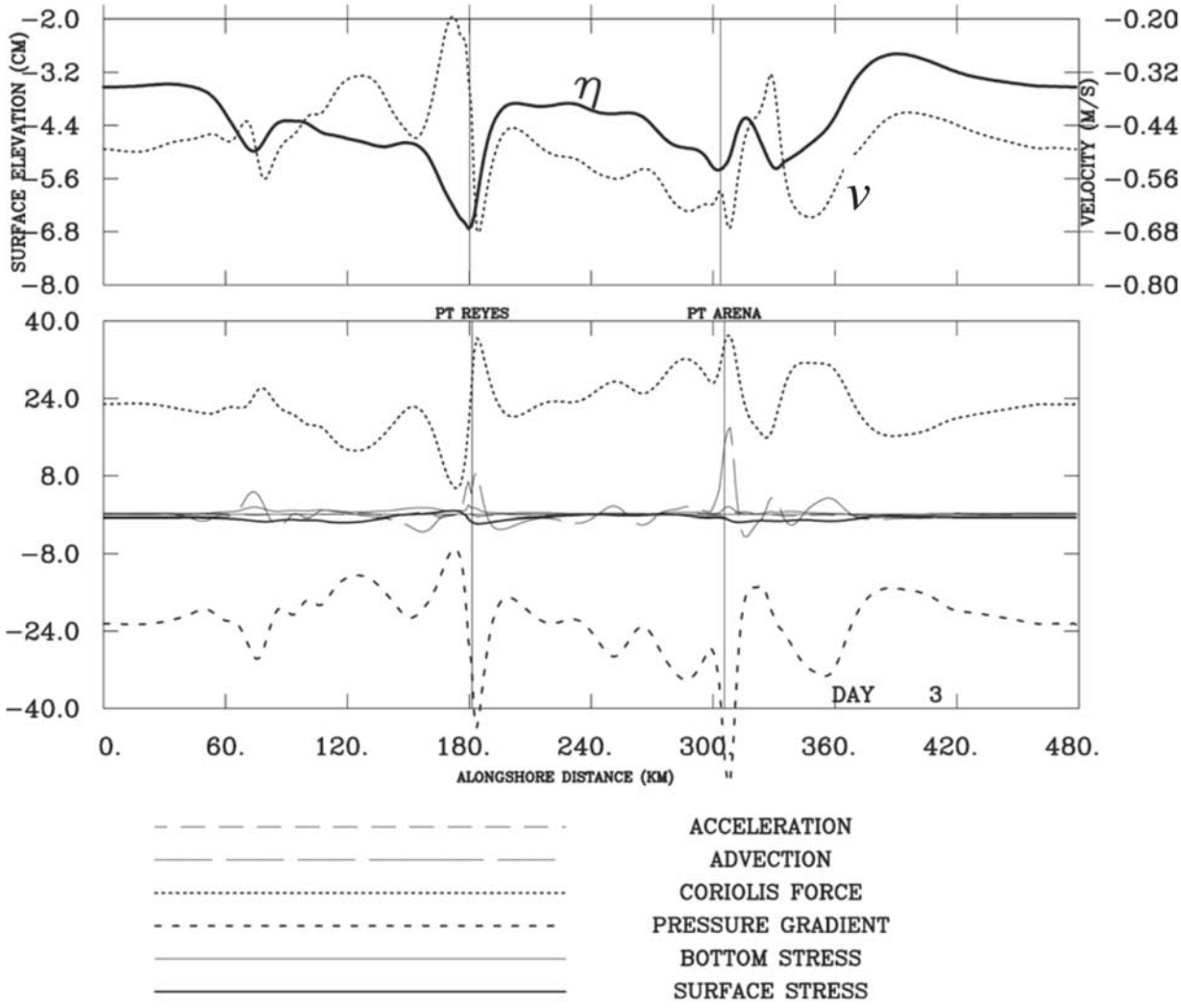

Figure 12. (top) Surface elevation η and surface velocity v and terms in the depth-averaged across-shore momentum equation (3) (m s^{-2}, averaged over 24 hrs, multiplied by 10^6) as a function of distance y along the coast from locations approximately 6 km offshore on day 3 (5.5 km offshore for η and v).

decrease in surface temperatures near the coast between Pt. Reyes and Pt. Arena (Figure 9a). This is presumably due to more effective upwelling in that region and the question of why that is so naturally arises. The direction of the spatially constant wind stress coincides with the direction of the coastline there (Figure 5a) while it is incident to the coastline at a small angle in the north and south. Stronger upwelling should be expected where the wind stress is aligned with the coast. That effect, however, does not appear to be the important determining factor in this case. An additional experiment (Appendix A) with the wind stress aligned with the offshore boundary, and hence with the north and south coastlines (Figure 3), results in essentially the same response as shown in Figure 9a.

[42] To help understand the reason for the lower surface temperatures between Pt. Reyes and Pt. Arena, we examine in Figure 18 the day 10 fields of σ_θ at the surface, $\Delta\sigma_\theta = \sigma_\theta - \sigma_\theta$ ($t = 0$) at the bottom, and the depth-averaged pressure gradient in the alongshore direction $\rho_0^{-1}\partial P/\partial y$ from equation (4). The surface σ_θ field shows the most dense surface water next to the coast around 38.4° and 38.7°N directly south of the smaller capes at about 38.6° and 38.8°N. In contrast, south of Pt. Reyes the surface σ_θ field shows a complex structure associated with the separation of the coastal current and the surface density values are not as high as found to the north. The $\Delta\sigma_\theta$ fields on the bottom have largest values next to the coast in regions similar to those of largest surface σ_θ but displaced several km northward. This is consistent with southward advection by alongshore currents influencing the upwelling process. The alongshore pressure gradient field is negative between Pt. Reyes and Pt. Arena over essentially the entire region in which the largest values of $\Delta\sigma_\theta$ and surface σ_θ are found. It appears, consequently, that the presence of negative pressure gradients remains an important factor in maintaining effective upwelling.

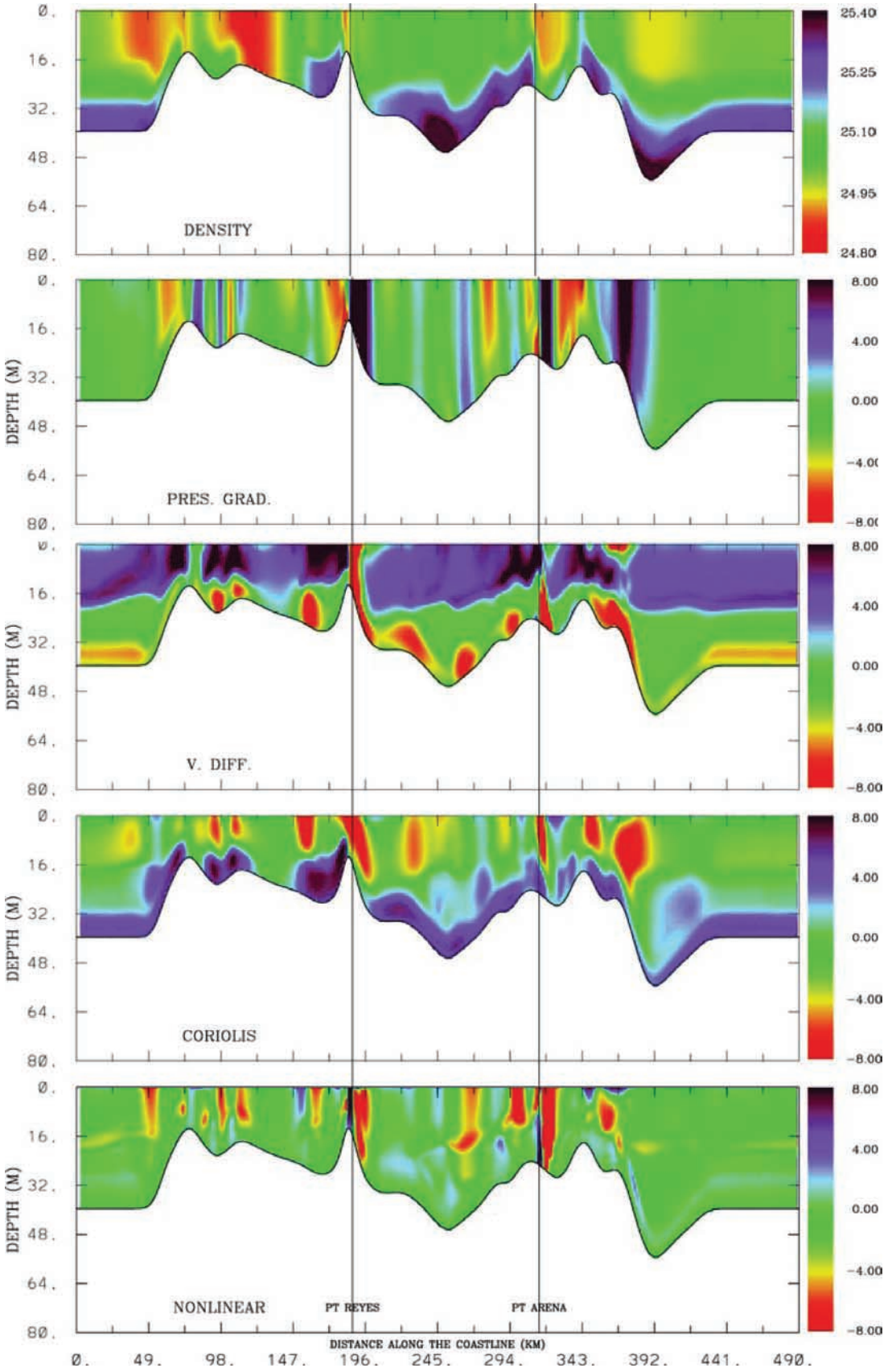

Figure 13. Potential density σ_θ (kg m^{-3}) and terms from the alongshore momentum equation (1): pressure gradient, vertical diffusion, Coriolis force, and nonlinear advection (m s^{-2}, averaged over 24 hrs, multiplied by 10^6) as a function of depth and distance along the coast at locations approximately 2.5 km offshore on day 3.

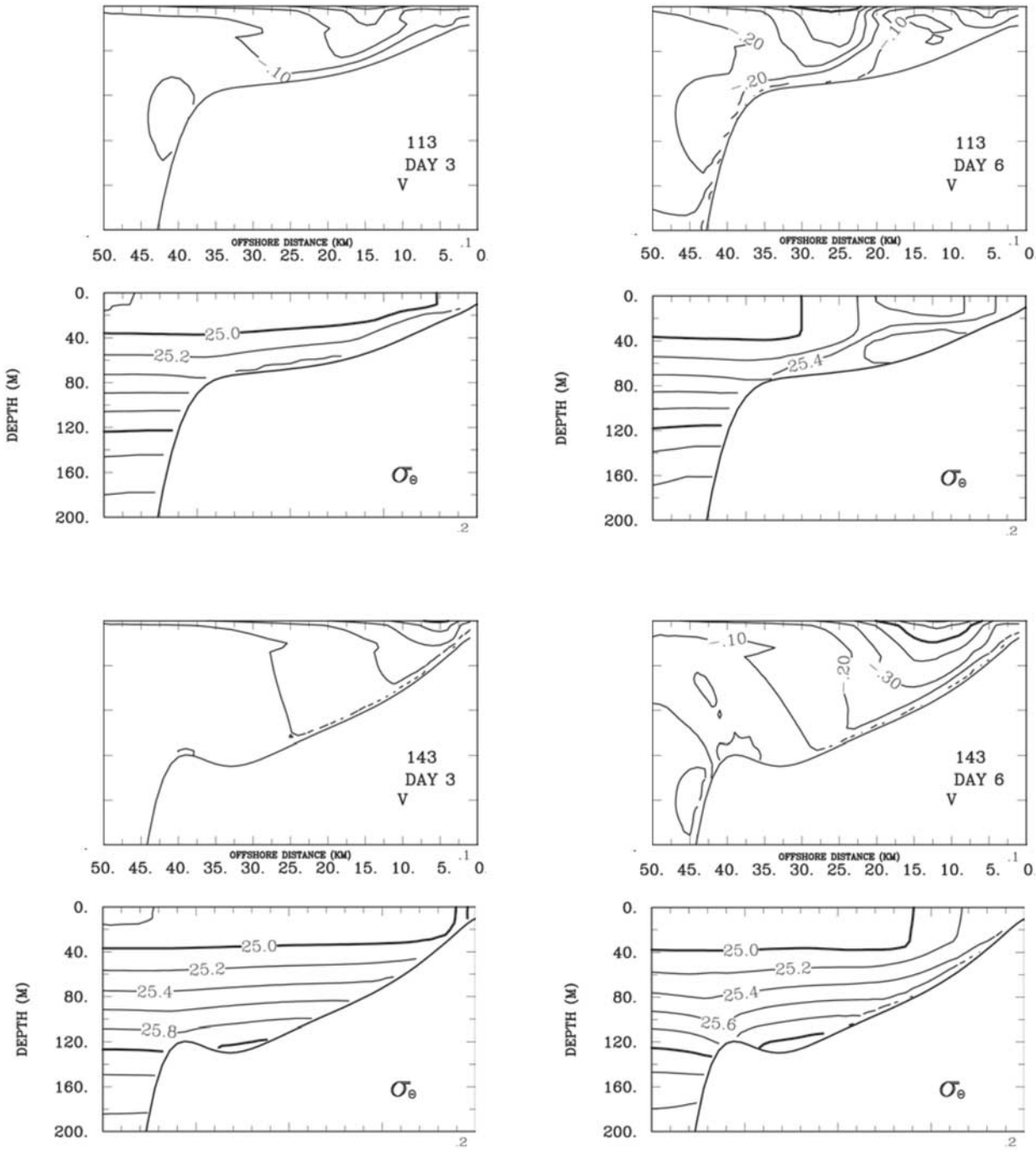

Figure 14. Across-shore sections of daily averaged alongshore velocity v (m s^{-1}) and potential density σ_θ (kg m^{-3}) at lines 113 and 143 on days 3 and 6. The contour intervals are 0.1 m s^{-1} for v and 0.2 kg m^{-3} for σ_θ.

[43] To investigate further the role of pressure gradients in the upwelling in this region, we examine the evolution of the shelf flow field at location 170 (Figure 18), which is positioned just south of the cape at 38.6°N in the region where on day 10 at the coast $\Delta\sigma_\theta$ on the bottom and the magnitude of the northward pressure gradient are near local maxima. Across-shelf sections of σ_θ and v at 170 on days 6, 10, 15 and 20 are shown in Figures 19 and 20, respectively. Also shown in those figures for comparison are corresponding sections from a separate calculation where the flow over the shelf/slope topography at 170 is forced by the local wind stress but is assumed to be two-dimensional, i.e., to have zero gradients in the alongshore direction. Terms from the z-dependent alongshore momentum balance (equation (1)) and vertical velocities w on the section at 170 for days 6 and 10 are plotted in Figure 21.

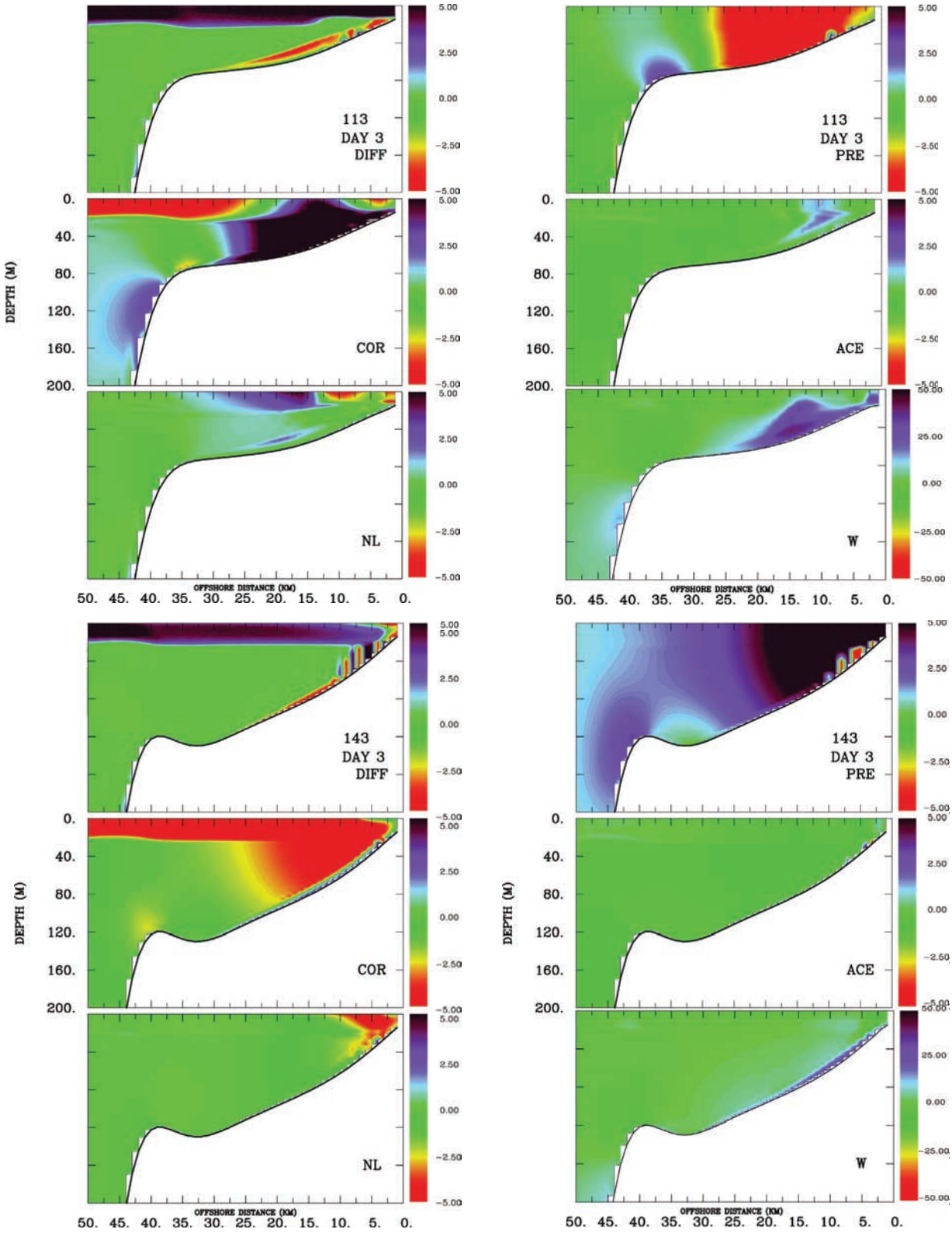

Figure 15. Across-shore sections of terms in the alongshore momentum equation (1) at lines 113 and 143 on day 3 (m s^{-1}, averaged over 24 hrs, multiplied by 10^6). DIFF: vertical diffusion; COR: Coriolis force; NL: nonlinear advection; PRE: pressure gradient; ACE: acceleration; and W: vertical velocity w ($\times 10^{-5}$ m s^{-1}).

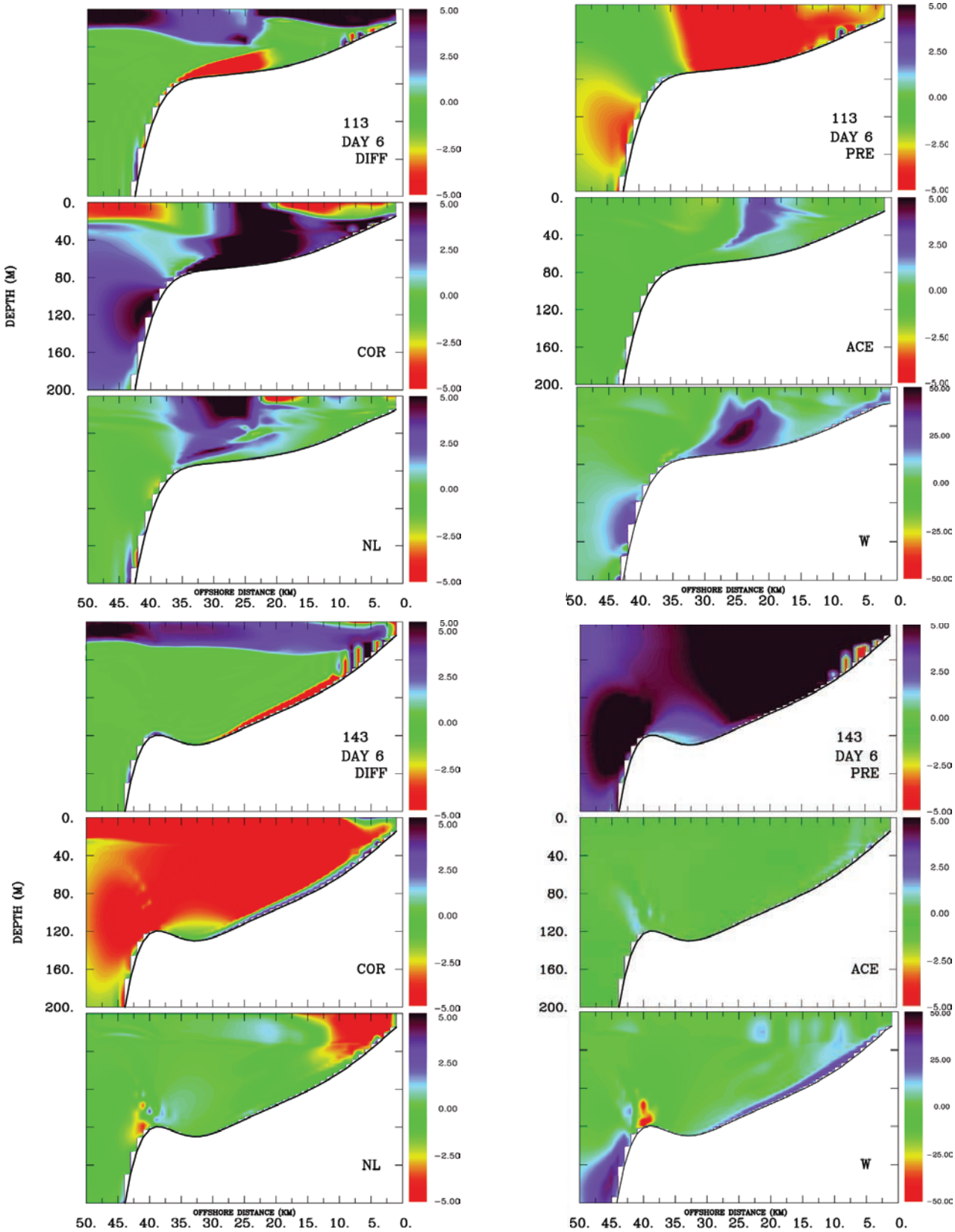

Figure 16. Across-shore sections of terms in the alongshore momentum equation (1) at lines 113 and 143 on day 6 (m s^{-1}, averaged over 24 hrs, multiplied by 10^6). DIFF: vertical diffusion; COR: Coriolis force; NL: nonlinear advection; PRE: pressure gradient; ACE: acceleration; and W: vertical velocity w ($\times 10^{-5}$ m s^{-1}).

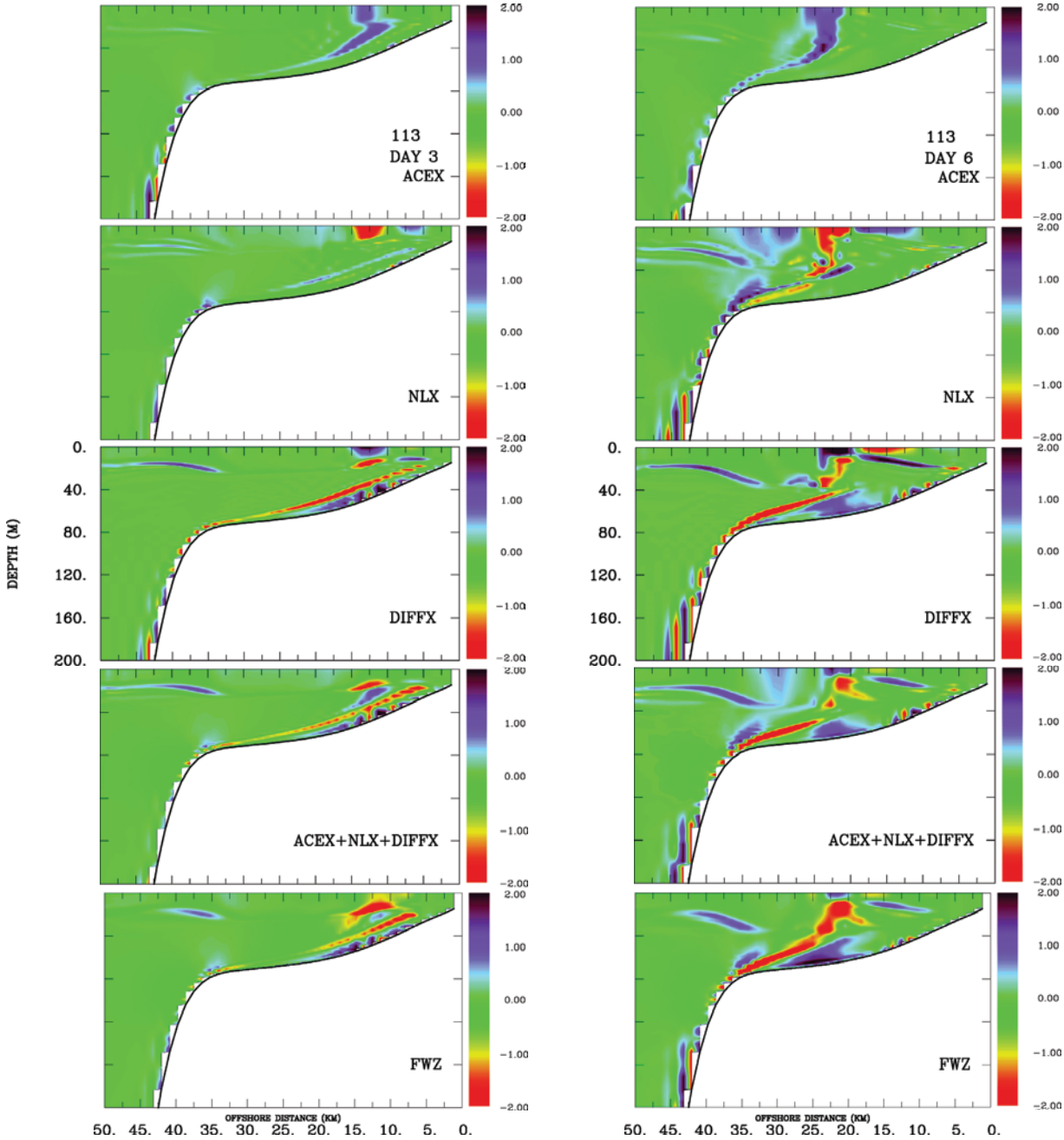

Figure 17. Across-shore sections of daily averaged terms (B12a), (B12b), and (B12c) in the approximate vorticity equation (B11) at line 113 on days 3 and 6. The terms are ACEX [v_{xt}], NLX [$(\mathbf{u}\cdot\nabla v)_x$], DIFFX [$-(K_M v_z)_{zx}$], the sum ACEX + NLX + DIFFX [$v_{xt} + (\mathbf{u}\cdot\nabla v)_x - (K_M v_z)_{zx}$] and *FWZ*[$fw_z$].

[44] A comparison of the σ_θ sections from 170 with those from the 170-2D solution on days 6 and 10 (Figure 19) shows larger values of σ_θ at the surface and at most depths below the surface over the shelf for 170. The alongshore velocities on days 6 and 10 are generally weaker, the core of the coastal jet is displaced farther offshore, and the near-bottom gradients are smaller for 170 compared to 170-2D. The terms in the alongshore momentum balances for 170 show positive vertical diffusion in a surface layer of depth about 30 m which is primarily balanced by a negative Coriolis force, corresponding to offshore flow in a surface Ekman layer. Over the shelf below the surface layer, the Coriolis force is positive corresponding to positive onshore flow. Positive vertical velocities are also found over the shelf. The location of the positive vertical velocities appear to be directly related to those of the stronger onshore flow. A negative pressure gradient balances the positive Coriolis force associated with the onshore flow at depth and also balances a positive nonlinear advection term near the surface over the shelf. The latter is most likely due to a positive

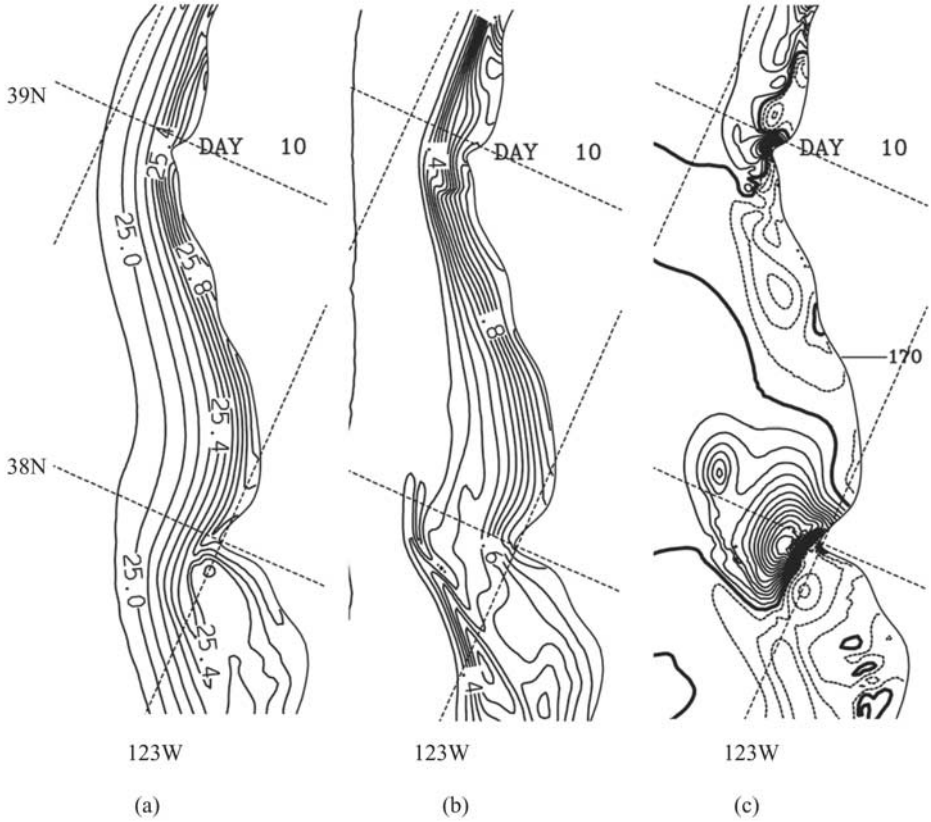

Figure 18. Daily averaged fields on day 10 of (a) σ_θ at the surface (interval 0.1 kg m^{-3}), (b) $\sigma_\theta - \sigma_\theta$ ($t = 0$) at the bottom (interval: 0.05 kg m^{-3}), and (c) depth-averaged y pressure gradient (multiplied by 10^6, interval 1 m s^{-2} with a heavy contour line for 0).

contribution from vv_y in this region south of the cape at 38.6N as indicated by the spatial variation of the surface velocity vectors in Figure 5a.

[45] Evidently it is the negative pressure gradient that leads, through balance of fu in place of v_t, to the generally weaker alongshore currents at 170 compared to 170-2D and in particular to the decreased alongshore currents near the coast at 170. In addition, the support of geostrophically balanced onshore flow below the surface layer by the negative pressure gradient at 170 appears to lead to stronger vertical velocities and correspondingly higher densities at middepth over the shelf. We expect also that the potential vorticity dynamics that plays a part in the upwelling in the separated coastal current south of Pt. Reyes is also operative to some extent between Pt. Reyes and Pt. Arena on days 6–10. The similarity lies in the presumably advectively driven slow offshore movement of the core of the coastal jet in this region as it appears to seek a straighter path between Pt. Arena and Pt. Reyes. In the 170-2D response on days 6 and 10, the onshore flow is largely restricted to the bottom boundary layer, the presence of which is indicated by the strong vertical gradients in v within about 20 m of the bottom.

[46] On day 15 near the coast and over the bottom part of the water column, northward currents, similar to those on the R line (Figure 7), are also found at section 170. By day 20 the northward currents have almost disappeared. The behavior of σ_θ and v from the 170-2D solution presents an interesting contrast. In the two-dimensional case, the day 15 and day 20 sections of both σ_θ and v are essentially unchanged, exhibiting only a slight decrease in the magnitude of v presumably caused by bottom frictional effects. The 170 sections, on the other hand, show considerable changes in the structure of σ_θ and of v on days 15 and 20. These changes reflect the three-dimensional, time-dependent response to upwelling wind relaxation events of the primarily pressure gradient driven shelf flow. The relatively large differences in the day 15 and day 20 v and σ_θ sections at 170 and at the C line (Figure 6), compared to the similar structure of those variables at the two sections on day 10, emphasize the fact that in addition to differing markedly from a two-dimensional situation, the three-dimensional shelf flow response to decreasing winds typically will have strong spatial variability directly dependent on the surrounding shelf topography.

[47] We note that our description of the three-dimensional shelf flow response to decreasing southward wind stress does not at all preclude the possibility of contributions from linear coastal-trapped wave dynamics to the adjustment process. The general complexity of the flow response and the relatively short alongshore scales involved, however,

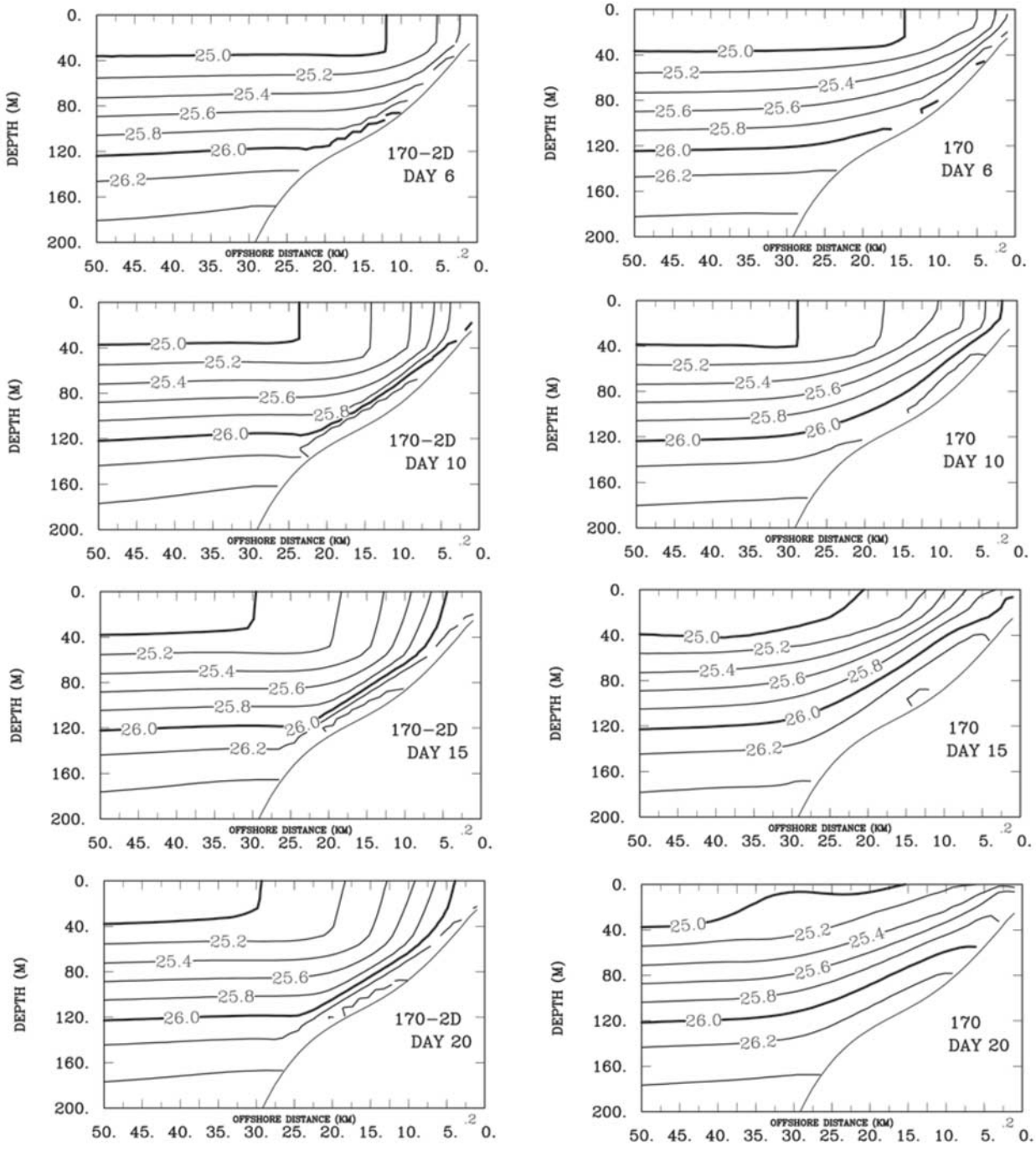

Figure 19. Across-shore sections of daily averaged potential density σ_θ (kg m^{-3}) at line 170 on days 6, 10, 15, and 20. (left) The solutions, designated 170-2D, are obtained from a corresponding two-dimensional calculation, as discussed in the text. Contour intervals are 0.2 kg m^{-3} with heavy contour lines for 25 and 26 kg m^{-3}.

have made it difficult to identify unambiguous signatures of the presence of coastal-trapped wave processes.

6. Discussion

[48] The model results from this study of shelf flow response to an idealized upwelling wind relaxation event show clearly that, after the cessation of southward winds, northward currents are forced on the inner shelf near the coast by negative pressure gradients. The pressure gradients are set up by the interaction of the wind-forced shelf flow with alongshore variations in the coastline and in the shelf bottom topography.

[49] Based on the analyses in sections 4 and 5, our interpretation of the dynamics involved in these shelf flow processes is the following. Alongshore velocities in the

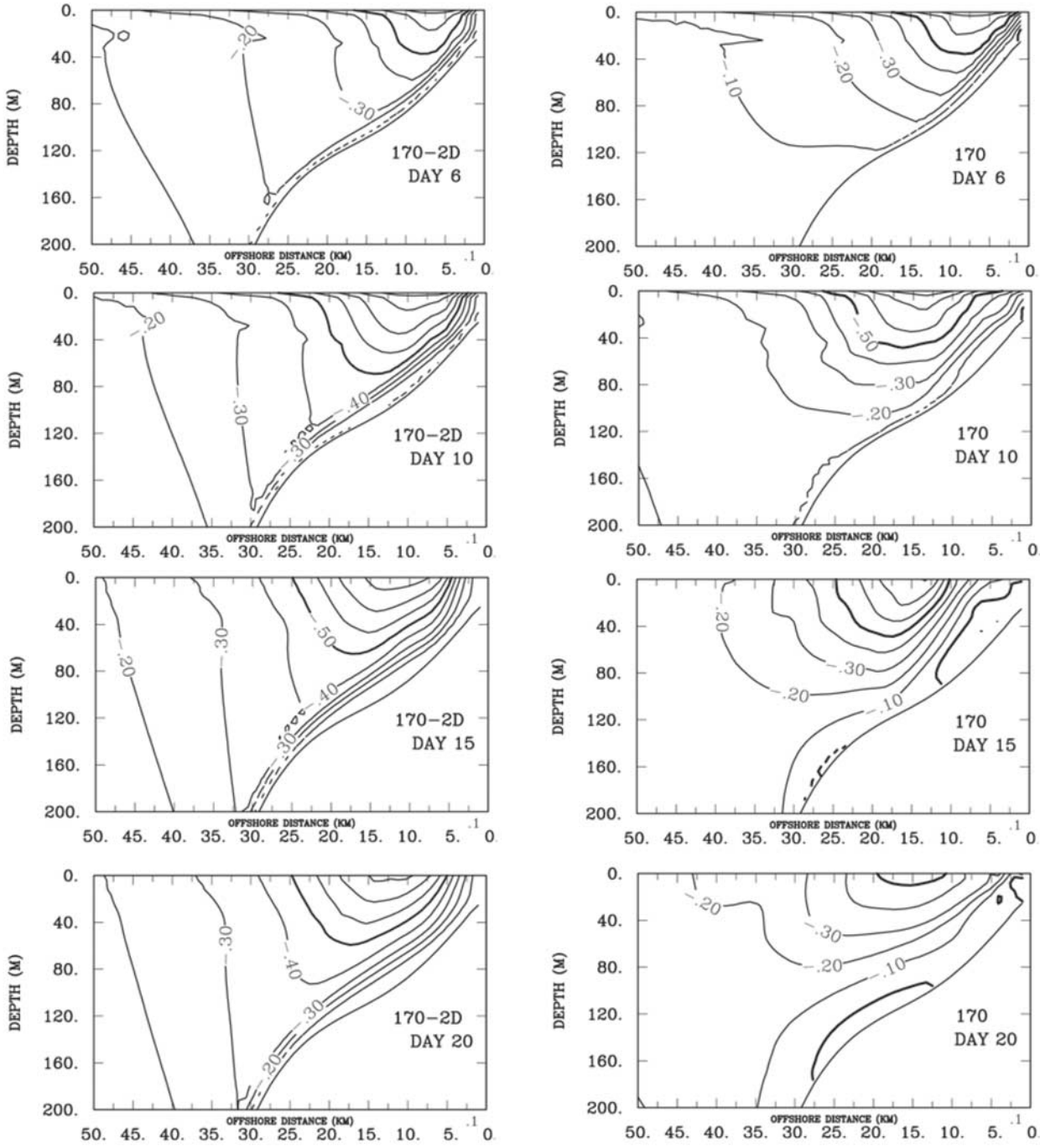

Figure 20. Across-shore sections of daily averaged alongshore velocity v (m s^{-1}) at section 170 on days 6, 10, 15, and 20. (left) The solutions, designated 170-2D, are obtained from a corresponding two-dimensional calculation as discussed in the text. Negative (positive) values of v are indicated by solid (dashed) contours. Contour intervals are 0.1 m s^{-1} with heavy contour lines for 0 and -0.5 m s^{-1}.

coastal jet increase in magnitude as the wind-forced coastal current flows around capes. As a consequence of this increase and of the geostrophic balance of the alongshore velocities, locally lower pressure develops at the coast near the location of the capes. In addition, at Pt. Reyes and Pt. Arena the increase in magnitude of v is sufficiently large to change the local balance in the across-shelf momentum equation from geostrophic to gradient wind (5.1). This leads to additional ageostrophic decreases in pressure at the coast near the cape. As a result, negative pressure gradients are set up south of capes while positive pressure gradients are set up to the north.

[50] The set up of negative pressure gradients south of capes is accompanied by the establishment at those locations of geostrophically balanced onshore flow over the

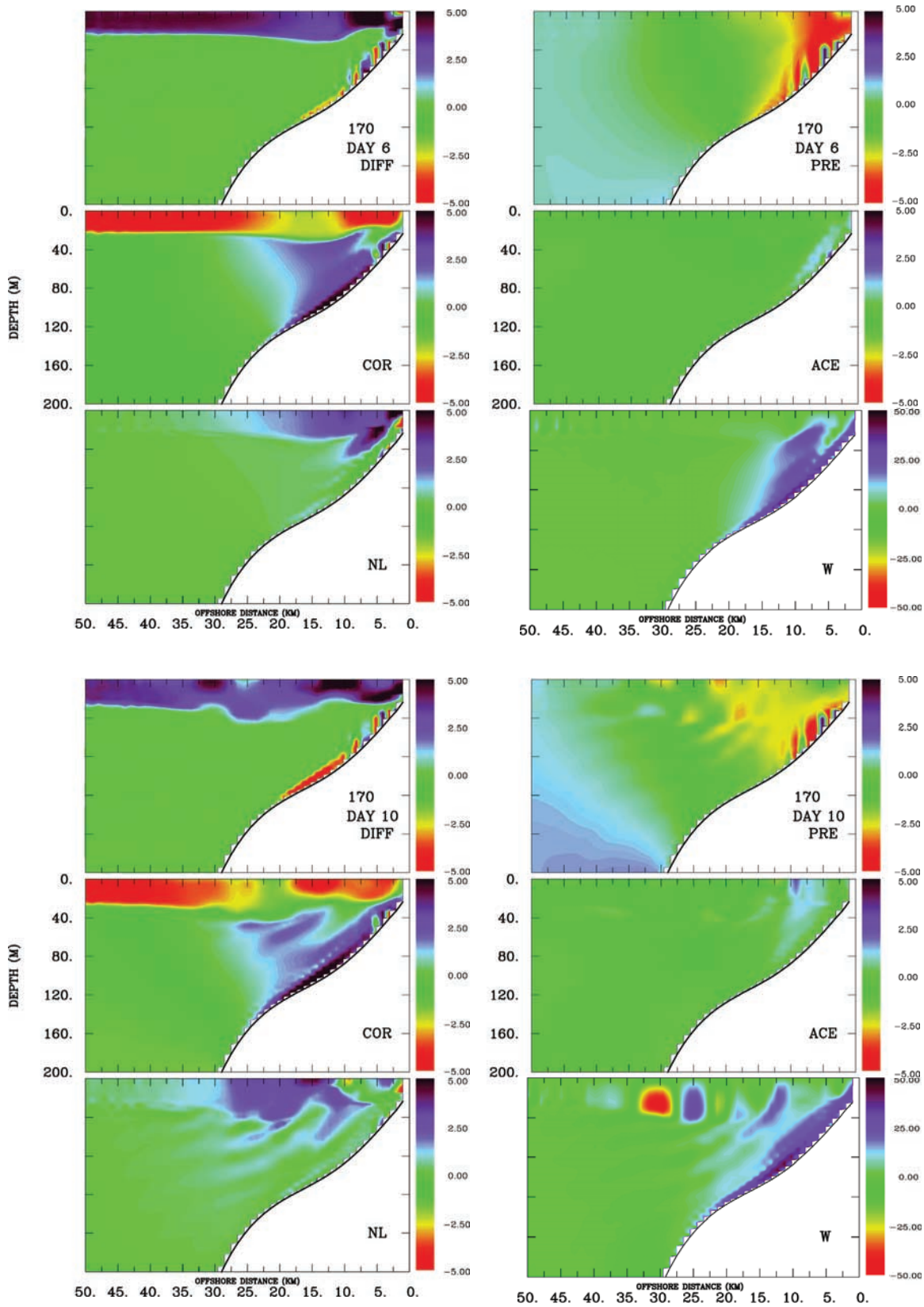

Figure 21. Across-shore sections of terms in the alongshore momentum equation (1) at line 170 for days 6 and 10 (m s^{-2}, averaged over 24 hrs, multiplied by 10^6). DIFF: vertical diffusion; COR: Coriolis force; NL: nonlinear advection; PRE: pressure gradient; ACE: acceleration; and W: vertical velocity w ($\times 10^{-5}$ m s^{-1}).

shelf throughout the water column. This onshore flow helps balance the wind-forced offshore mass flux in the surface Ekman layer and is accompanied by positive vertical velocities also over much of the water column on the inner shelf. The positive vertical motion advects the density field upward and increases the density of the water at depths over the shelf. The location and structure of the vertical velocities appear to be influenced by potential vorticity dynamics associated with the separation of the alongshore coastal current south of capes.

[51] In contrast, to the north of the capes the positive pressure gradient, in addition to involvement in geostrophic balance of offshore flow, also contributes strongly to the balance of negative nonlinear advective effects associated with the spatial acceleration of the coastal current as it flows toward the capes. The wind-forced offshore flow in the surface layer north of capes is primarily balanced by onshore flow in a bottom Ekman layer. One net result of these differences in flow processes north and south of capes is the enhancement of the effectiveness of upwelling in bringing dense water to the surface over the shelf near the coast to the south of capes.

[52] When the southward wind stress decreases, the forcing of offshore flow in the surface layer and the requirement for compensating onshore flow also decrease. The negative pressure gradients that balanced the forced onshore flow remain, however. As the wind-forced across-shelf circulation weakens, the negative pressure gradients accelerate alongshore currents northward. The positive pressure gradients to the north of capes, on the other hand, evidently remain primarily in a balance with the negative nonlinear advection in the coastal jet, which tends to move offshore. Hence, the positive pressure gradients are not made free by the cessation of the wind stress to accelerate currents southward in the same manner as the northward gradients accelerate currents northward. We attribute the clear dominance of northward currents near the coast over much of the domain after day 17 (Figure 9b) to this difference in response to northward and southward pressure gradients.

[53] It is important to recall that the forcing in these experiments involves spatially uniform wind stress and no surface heat flux. Thus the alongshore pressure gradients are set up solely by the interaction of the wind-driven currents with shelf topography and not by specific alongshore variations in atmospheric forcing. It appears, consequently, that pressure gradient driven northward currents are likely to be a robust characteristic of U.S. west coast shelf flow response to time variable upwelling winds. In addition, the results demonstrate that the nature of three-dimensional, time-dependent, stratified, shelf flow interactions with topography is complex. Increased understanding of these processes is clearly desirable and will require considerable additional studies beyond the initial analyses presented here.

Appendix A. Additional Experiments

[54] We investigate first the sensitivity of the results of the basic case experiment to variations in the specification of the forcing with additional numerical experiments. The objective is to examine the robustness of the response found in the basic case experiment. To facilitate the completion of experiments for this purpose, we have used a grid with reduced resolution ($\Delta x \simeq 2$ km, 30 sigma levels). A repeat of the basic case experiment (denoted BC) with the reduced resolution grid (denoted BC-RG) gives results that are close to those obtained with the high resolution grid. Consequently, we feel confident that, for these purposes, the experiments with the reduced resolution grid give meaningful comparisons.

[55] Results from only two relevant additional experiments are reported here for brevity. In one (denoted NS WIND), the direction of the wind stress is taken as 335.5°T so that the wind stress is aligned with the offshore boundary of the grid (Figure 3) and thus with the coastline to the north and south. In the second experiment (denoted 5 DAY), the wind stress is aligned as in BC and BC-RG, but is maintained at 0.1 Pa for 5 days, rather than 10 days as in BC, before decreasing to zero in a similar manner over 3 days.

[56] The alongshore velocity v and surface temperature T from the experiments (BC-RG, NS WIND, 5 DAY) are plotted in Figure A1 as a function of y at a location approximately 3 km from the coast for days (10,10,5), respectively, just before the upwelling favorable wind stress starts to decrease. The same variables are also plotted 5 days after the wind stress starts to decrease on days (15,15,10), respectively.

[57] The alongshore structure of v and T from the BC-RG and NS WIND experiments, are qualitatively similar with each other and also with BC on both days 10 and 15. In particular, similar low temperatures between Pt. Reyes and Pt. Arena on day 10 and similar northward currents in a region from south of Pt. Reyes to north of Pt. Arena on day 15 are evident. The close comparison of these results indicates that the alignment of the wind stress along 317°T in BC is not the important factor in leading to the qualitative nature of the day 10 alongshore structure of the surface temperatures with lowest temperatures between Pt. Reyes and Pt. Arena.

[58] The day 5 structures of v and T from the 5 DAY experiment are similar to those found in BC on day 5 (Figure 9a). Of relevance in this experiment, is the fact that on day 10 northward currents are found between Pt. Reyes and Pt. Arena. Similar results are found in additional experiments with the duration of the constant wind stress varied between 5 and 15 days. These results indicate that the presence of a northward current generation mechanism following weakening of upwelling favorable winds does not depend with great sensitivity on the exact duration chosen for the upwelling winds in BC.

[59] Second, we briefly compare the results from the basic case experiment (BC-RG) with those from some additional experiments with reduced physics and with simplified topography. The reduced resolution grid is used for these experiments also. In the reduced physics experiment, we utilize a linear version of the model produced by

Figure A1. (opposite) Daily averaged values of surface alongshore velocity and surface temperature as a function of distance y along the coast from locations approximately 3 km offshore from experiments BC-RG, NS WIND, and DAY 5 for (top) days 10,10, and 5 and (bottom) days 15, 15, and 10, respectively.

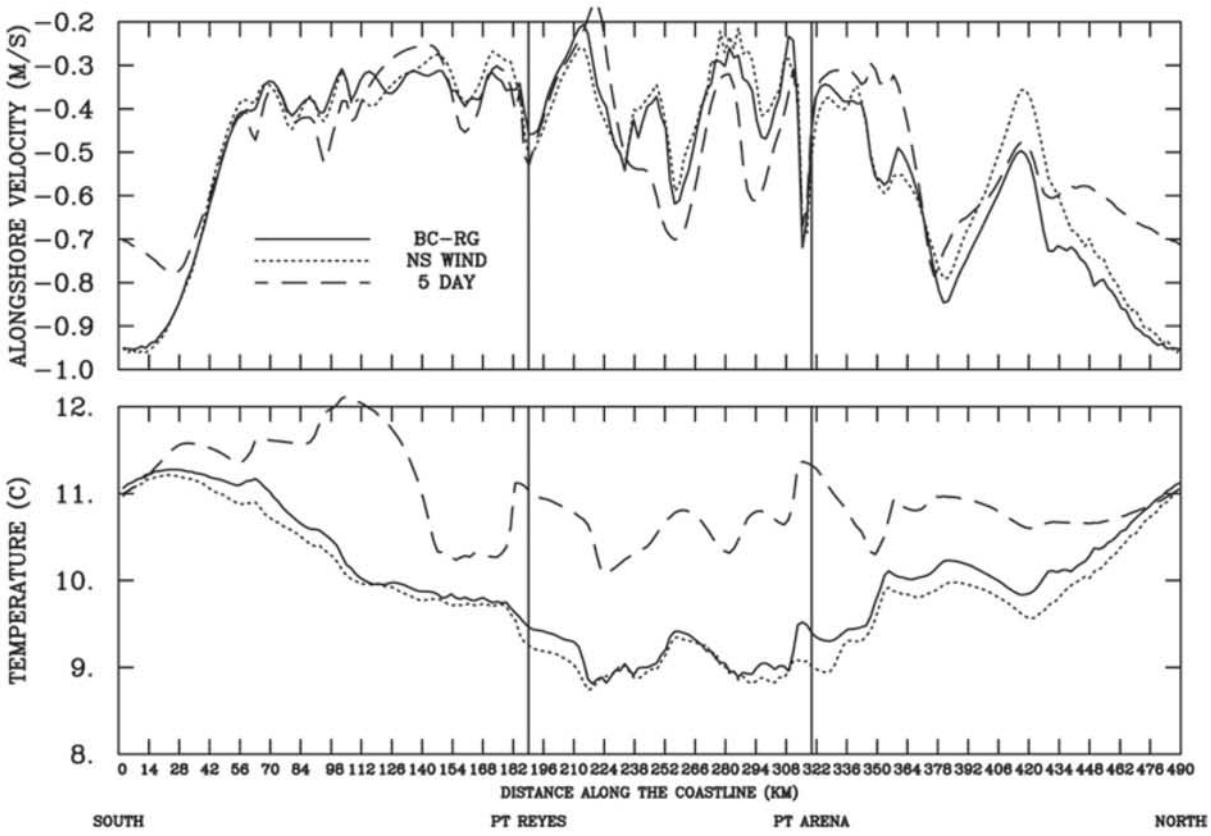
ALONGSHORE VELOCITY (M/S)
−0.2
−0.3
−0.4
−0.5
−0.6
−0.7
−0.8
−0.9
−1.0
BC−RG
NS WIND
5 DAY
TEMPERATURE (C)
12.
11.
10.
9.
8.
0 14 28 42 56 70 84 98 112 126 140 154 168 182 196 210 224 238 252 266 280 294 308 322 336 350 364 378 392 406 420 434 448 462 476 490
DISTANCE ALONG THE COASTLINE (KM)
SOUTH
PT REYES
PT ARENA
NORTH

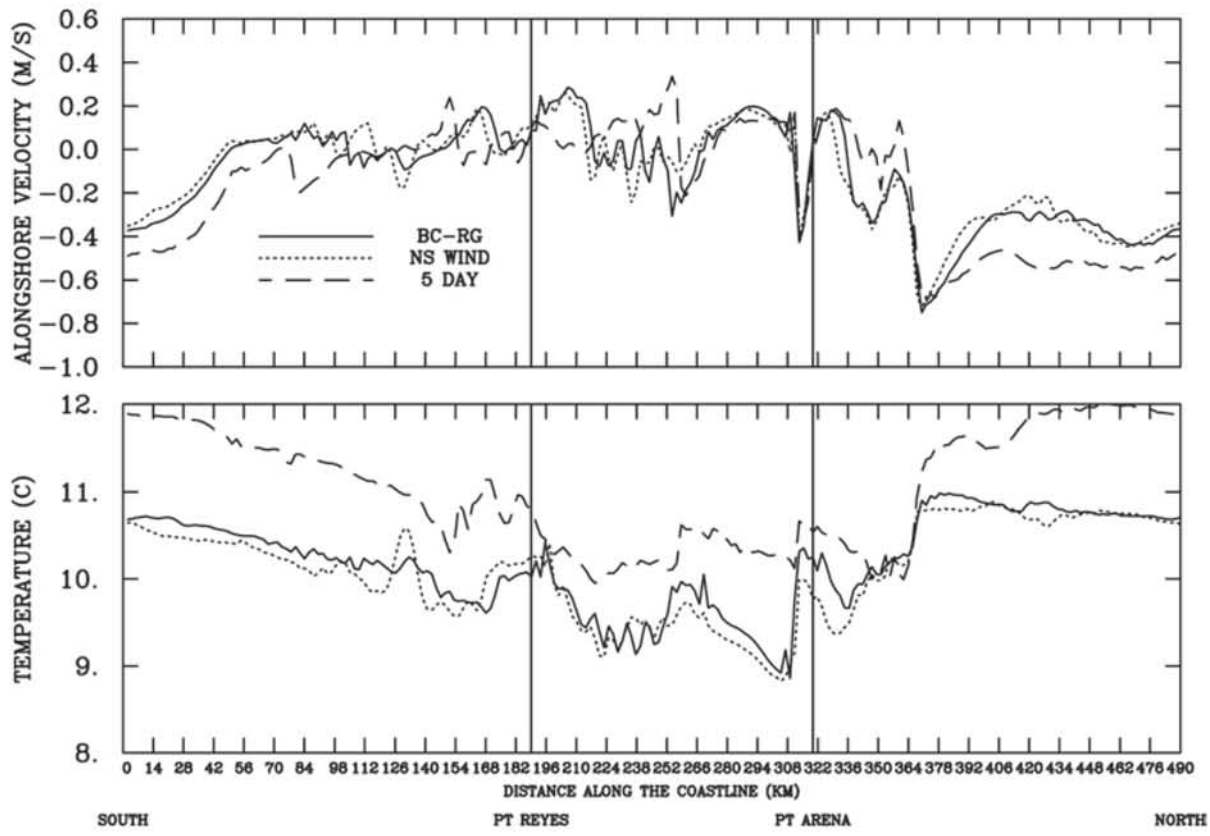
ALONGSHORE VELOCITY (M/S)
0.6
0.4
0.2
0.0
−0.2
−0.4
−0.6
−0.8
−1.0
BC−RG
NS WIND
5 DAY
TEMPERATURE (C)
12.
11.
10.
9.
8.
0 14 28 42 56 70 84 98 112 126 140 154 168 182 196 210 224 238 252 266 280 294 308 322 336 350 364 378 392 406 420 434 448 462 476 490
DISTANCE ALONG THE COASTLINE (KM)
SOUTH
PT REYES
PT ARENA
NORTH

removing the nonlinear advection terms in the momentum equations and by using the initial horizontally uniform depth-dependent T and S fields in the advection terms in the T and S equations, respectively. The other conditions, e.g., forcing, topography, etc., in this experiment (denoted as LIN) are identical to those in the basic case experiment (BC-RG). The objective is to provide a simple direct illustration of the effects on nonlinear advective processes in the basic case.

[60] In the simplified topography case, we utilize the full equations in a flat bottom region of depth 300 m with a vertical wall coast along the same variable coastline as in the basic case. The idealization of a flat bottom shelf with a vertical wall is frequently utilized in simplified coastal models to provide insight into the flow response near a coastal boundary. The objective here is to briefly compare results of that idealization, which omits shelf and slope bottom topography but retains coastline variability, with those from the basic case experiment. In this experiment (denoted as FB), the forcing, the initial stratification (down to 300 m) and the other conditions are the same as in the basic case. To be in closer agreement with possible laboratory experiments involving vertical walls, however, the boundary condition on the tangential component of the velocity at the coast is changed to no slip, i.e., to $v = 0$. We note that results that are qualitatively similar to those shown here for the FB experiment are obtained utilizing flat bottom depths of 100 m and 200 m, with the shallower depths resulting, as expected, in generally larger magnitude wind-forced depth-averaged currents and also, after the wind ceases, in larger depth-averaged current deceleration rates due to bottom friction.

[61] Depth-averaged velocity vectors in the vicinity of the Pt. Reyes on days 10 and 15 from experiments BC-RG, LIN and FB are plotted in Figure A2. Also shown are the day 15 minus day 10 difference vectors. In LIN the coastal jet on day 10 flows along the coast past Pt. Reyes without the offshore deflection or separation found in BC-RG. The near-coastal southward alongshore currents are correspondingly stronger in LIN south of Pt. Reyes. On day 15, the near coastal currents in LIN are reduced considerably in magnitude, but remain southward. This reduction in magnitude, shown clearly by the northward day 15 minus day 10 difference vectors, is caused by a positive northward acceleration of V near the coast. An examination of term balances in the depth-integrated alongshore momentum equation shows that this acceleration is balanced, to the south and farther north of Pt. Reyes, by negative pressure gradients and, directly off Pt. Reyes, by bottom friction. Nevertheless, in LIN the overall day 15 flow pattern remains qualitatively similar to that on day 10. This behavior is in contrast to that in BC-RG where on day 15 the development of northward currents near the coast off Pt. Reyes and the strengthening of a cyclonic eddy south of Pt. Reyes are evident. The day 15 minus day 10 difference velocity vectors from BC-RG near the coast are generally stronger northward than those from LIN. These variations in strength of the difference vectors, together with the fact that on day 10 the currents next to the coast in LIN are generally stronger southward, are consistent with the presence on day 15 of northward currents next to the coast in BC-RG and with no northward currents in LIN. Overall the considerable differences in the BC-RG and the LIN velocity fields demonstrate the importance of nonlinear advection effects in determining the behavior of the day 10 wind forced shelf flow in the vicinity of Pt. Reyes and in influencing the day 15 response of near-coastal currents to the wind relaxation. Contributions of nonlinear advective effects in the basic case experiment BC, identified through momentum and vorticity term balances, are discussed in sections 4 and 5.

[62] In FB, separation of the coastal current and formation of a cyclonic eddy south of Pt. Reyes is observed on day 10. The day 15 minus day 10 difference velocity vectors, however, are generally considerably smaller in magnitude than the difference velocity vectors found in BC-RG or in LIN. Near the coast the difference vectors in FB are weakly northward offshore and to the north of Pt. Reyes, but are extremely small south of Pt. Reyes. To investigate possible effects from variations in response time between BC-RG and the flat bottom case FB, difference velocity vectors were examined for a set of days 14–20 minus day 10. Qualitative conclusions from those comparisons were identical. Overall, an assessment of the differences in the results from FB and from BC-RG indicates that, although separation is found south of Pt. Reyes on day 10 in both experiments, the shelf and slope topography is clearly important in determining major qualitative aspects of the response of coastal currents to variable wind forcing. The effects of alongshore variations in coastline and in shelf topography accompany each other and clearly act together in influencing the behavior of shelf flow fields.

Appendix B. Approximate Potential Vorticity Dynamics

[63] In order to help understand the behavior of the shelf flow response, we examine the inviscid vorticity dynamics of an approximate system of equations. Based on the results of the numerical solutions (e.g., Figure 12), we assume that the alongshore velocity is in geostrophic balance. It is convenient to use Cartesian coordinates (x,y,z). The approximate equation set is

$$u_x + v_y + w_z = 0, \tag{B1a}$$

$$fv = p_x/\rho_0, \tag{B1b}$$

$$v_t + \mathbf{u}\cdot\nabla v + fu = -p_y/\rho_0, \tag{B1c}$$

$$0 = -p_z - \rho g, \tag{B1d}$$

$$\rho_t + \mathbf{u}\cdot\nabla\rho = 0, \tag{B1e}$$

where subscripts (x,y,z,t) denote partial differentiation, the velocity vector $\mathbf{u}$ has components (u,v,w), ρ is the perturbation potential density, and, e.g., $\mathbf{u}\cdot\nabla\rho = u\rho_x + v\rho_y + w\rho_z$. This system of equations is similar to a restricted version of the geostrophic momentum approximation of *Hoskins* [1975].

[64] Equations (B1a), (B1b), and (B1d) imply the thermal wind equation

$$fv_z = -g\rho_x/\rho_0. \tag{B2}$$

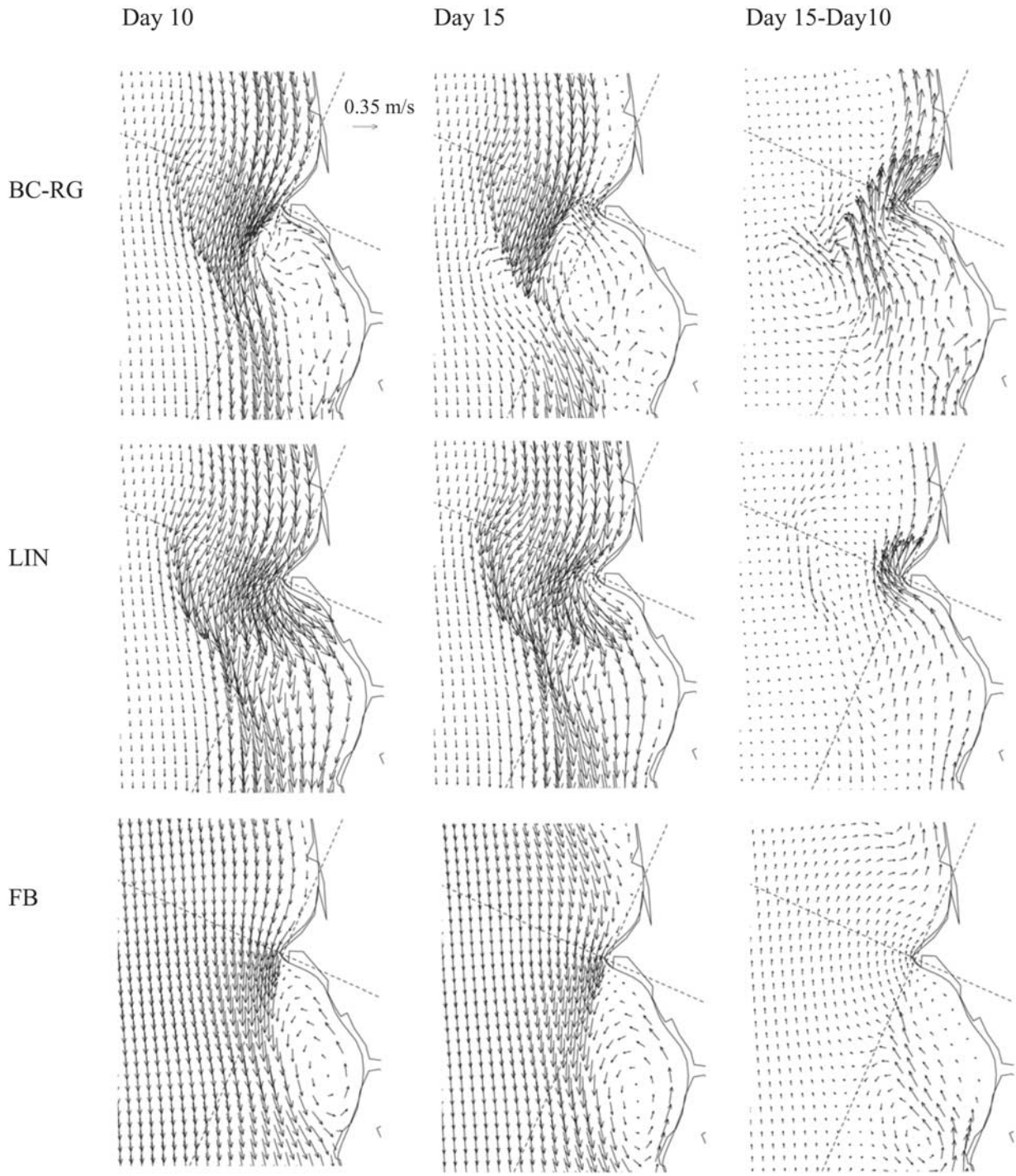

Figure A2. Depth-averaged velocity vectors in the vicinity of Pt. Reyes on days 10 and 15 from experiments BC-RG, LIN, and FB. Also shown are the corresponding day 15 minus day 10 differences of the depth-averaged velocity vectors.

A vorticity equation may be derived by adding the x derivative of equation (B1c) to the y derivative of equation (B1b) and using equation (B1a):

$$v_{xt} + (\mathbf{u} \cdot \nabla v)_x = f w_z. \tag{B3}$$

[65] The equations (B1) conserve potential vorticity

$$q = -v_z \rho_x + (v_x + f)\rho_z, \tag{B4a}$$

on fluid particles, i.e.,

$$q_t + \mathbf{u} \cdot \nabla q = 0. \tag{B4b}$$

[66] It follows from the addition of $f(B1c)_z + (g/\rho_0)\,(B1e)_x$ and the use of equations (B1a) and (B2) that

$$w_{zz} + \left(\frac{N^2}{f(f+v_x)} w_x\right)_x - 2\left(\frac{v_z}{(f+v_x)} w_z\right)_x = Q_x^{(x)}, \tag{B5}$$

where

$$Q^{(x)} = \frac{2}{f(f+v_x)}\frac{g}{\rho_0}\left(v_x\rho_y - v_y\rho_x\right), \tag{B6}$$

and $N^2 = -g\rho_z/\rho_0$.

[67] Thus, with v and ρ given in terms of p by equations (B1b) and (B1d), respectively. Equations (B1a), (B1b), (B1d), (B4), and (B5) comprise a governing equation set in one unknown variable p. The important points are that potential vorticity conservation (equations (B4b)) provides a single prognostic equation for q that, together with appropriate boundary conditions, determines p and that the velocity component w obeys a diagnostic, nonlinear, elliptic (for $fq < 0$) equation (B5).

[68] To better appreciate the implications of equation (B5) in a coastal upwelling context, we note that if, for example, the flow is two-dimensional with uniformity in y, i.e., $v_y = \rho_y = 0$, then a stream function may be defined such that

$$w = -\psi_x, \quad u = \psi_z, \tag{B7}$$

and equation (B5) reduces to

$$\psi_{zz} + \frac{N^2}{f(f+v_x)}\psi_{xx} - 2\frac{v_z}{(f+v_x)}\psi_{xz} = 0, \tag{B8}$$

with no inhomogeneous forcing terms on the right hand side. If further the flow is assumed to obey a linear approximation, equation (B8) reduces to

$$\psi_{zz} + \left(N^2/f^2\right)\psi_{xx} = 0 \tag{B9}$$

The nature of solutions to equation (B8), with boundary conditions relevant to the onset of upwelling in an idealized geometry, have been discussed by *Pedlosky* [1978]. Corresponding solutions to equation (B9) for upwelling in the linear approximation were given by *Allen* [1973].

[69] For three-dimensional flow fields, the nonlinear inhomogeneous terms $Q_x^{(x)}$ on the right hand side of equation (B5) play a role in determining the (x,z) structure of w. This situation is closely analogous to the recovery of the vertical velocity w from the omega equation in the quasi-geostrophic approximation [e.g., *Hoskins et al.*, 1978]. Here it is the x derivative of $Q^{(x)}$ that forces vertical motion in analogy with the divergence of the **Q** vector given by *Hoskins et al.* [1978].

[70] In trying to assess the impact of potential vorticity dynamics on the vertical velocity w over the shelf from the numerical solutions of the primitive equations in sigma coordinates, the multiple Cartesian coordinate derivatives in the terms on the right-hand side of equation (B5) make their meaningful numerical evaluation problematic. Consequently, we consider instead the term balances in the approximate vorticity equation (B3). In that way we can at least examine the contribution of the nonlinear term $(\mathbf{u}\cdot\nabla v)_x$ in balancing fw_z In addition, because of the importance on the shelf of frictional surface and bottom boundary layers, it is useful to include the effects of vertical diffusion in equation (B3). We do this in an approximate manner by assuming, in place of equations (B1b) and (B1c), that

$$fv = p_x/\rho_0 - (K_M u_z)_z \tag{B10a}$$

$$v_t + \mathbf{u}\cdot\nabla v + fu = -p_y/\rho_0 + (K_M v_z)_z \tag{B10b}$$

with $K_M = K_M(z)$. Further, we assume that $|v_x| \gg |u_y|$ in which case the resulting approximate vorticity equation, in place of equation (B3), is

$$v_{xt} + (\mathbf{u}\cdot\nabla v)_x - (K_M v_z)_{zx} = fw_z. \tag{B11}$$

[71] To evaluate the terms in equation (B8) from the numerical solution, we take the Cartesian coordinate x derivative of the corresponding terms in the sigma coordinate alongshore momentum equation (1). That is we find the terms by calculating

$$v_{xt} \simeq \frac{\partial}{\partial x_C}\left\{H^{-1}\frac{\partial(vD)}{\partial t}\right\}, \tag{B12a}$$

$$(\mathbf{u}\cdot\nabla v)_x \simeq \frac{\partial}{\partial x_C}\left\{H^{-1}\left[\frac{\partial(uD)}{\partial x} + \frac{\partial(v^2D)}{\partial y} + \frac{\partial(v\omega)}{\partial\sigma}\right]\right\}, \tag{B12b}$$

$$-(K_M)_{zx} \simeq -\frac{\partial}{\partial x_C}\left\{H^{-1}\frac{\partial}{\partial\sigma}\left(\frac{K_M}{D}\frac{\partial v}{\partial\sigma}\right)\right\}, \tag{B12c}$$

$$fw_z \simeq \frac{f\partial}{H\partial\sigma}w, \tag{B12d}$$

where the derivatives on the right-hand side in equation (B12) are in (x,y,σ) sigma coordinates, w is calculated consistently using (u,v,ω) and the definition of ω [*Blumberg and Mellor*, 1987], and where

$$\frac{\partial v}{\partial x_C} = \frac{\partial v}{\partial x} - \frac{\partial v}{\partial\sigma}\left(\frac{\sigma}{H}\frac{\partial H}{\partial x} + \frac{1}{H}\frac{\partial\eta}{\partial x}\right), \tag{B13}$$

gives the x derivative in Cartesian coordinates (with the assumption $D \simeq H$). We refer to the terms (B12a),(B12b), and (B12c) in the approximate vorticity equation (B11) as time rate of change, nonlinear, and vertical diffusion terms, respectively.

[72] **Acknowledgments.** This research was supported by the National Science Foundation Coastal Ocean Processes (CoOP) Program under grants OCE-9711481 and OCE-9907854. The authors gratefully acknowledge helpful discussions with J. Barth, R. Samelson, S. Lentz, P. Oke, and P. Newberger.

References

Allen J. S., Upwelling and coastal jets in a continuously stratified ocean, *J. Phys. Oceanogr.*, *13*, 245–257, 1973.

Beardsley R. C., and S. J. Lentz, The Coastal Ocean Dynamics Experiment collection: An introduction, *J. Geophys. Res.*, *192*, 1455–1463, 1987.

Blumberg A. F., and G. L. Mellor, A description of a three-dimensional coastal ocean circulation model, in *Three-Dimensional Coastal Ocean Models, Coastal Estuarine Sci.*, vol. 4, edited by N. Heaps, pp. 1–16, AGU, Washington D.C., 1987.

Gan J., and J. S. Allen, A modeling study of shelf circulation off northern California in the region of the Coastal Ocean Dynamics Experiment, 2, Simulations and comparisons with observations, *J. Geophys. Res.*, *107*, 10.1029/2001JC001190, 2002.

Holton J. R., *An Introduction to Dynamic Meteorology*, 3rd ed., 511 pp., Academic, San Diego, Calif., 1992.

Hoskins B. J., The geostrophic momentum approximation and the semi-geostrophic equations, *J. Atmos. Sci.*, *32*, 233–242, 1975.

Hoskins B. J., I. Draghici, and H. C. Davies , A new look at the ω-equation, *Q. J. R. Meteorol. Soc.*, *104*, 31–38, 1978.

Huyer A., and P. M. Kosro, Mesoscale surveys over the shelf and slope in the upwelling region near Pt. Arena, California, *J. Geophys. Res.*, *92*, 1955–1981, 1987.

Kosro P. M., Structure of the coastal current field off northern California during the Coastal Dynamics Experiment, *J. Geophys. Res.*, *92*, 1637–1654, 1987.

Levitus S., and R. Gelfeld, *NODC Inventory of Physical Oceanographic Profiles, Key to Oceanographic Records Documentation*, vol. 18, Natl. Oceanogr. Data Cent., Washington D.C., 1992.

Limeburner R., (Ed.), CODE-2 moored array and large-scale data report, *WHOI Tech. Rep. 85–35, CODE Tech. Rep. 38*, Woods Hole Oceanogr. Inst., Woods Hole, Mass., 1985.

Mellor G. L., and T. Yamada, Development of a turbulence closure model for geophysical fluid problems, *Rev. Geophys.*, *20*, 851–875, 1982.

Orlanski I., A simple boundary condition for unbounded hyperbolic flows, *J. Comput. Phys.*, *21*, 251–269, 1976.

Pedlosky J., A nonlinear model of the onset of upwelling, *J. Phys. Oceanogr.*, *18*, 178–187, 1978.

Send U., R. C. Beardsley, and C. D. Winant, Relaxation from upwelling in the Coastal Ocean Dynamics Experiment, *J. Geophys. Res.*, *92*, 1683–1698, 1987.

Winant C. D., R. C. Beardsley, and R. E. Davis, Moored wind, temperature, and current observations made during Coastal Ocean Dynamics Experiments 1 and 2 over the northern California Continental Shelf and upper slope, *J. Geophys. Res.*, *92*, 1569–1604, 1987.

J. S. Allen and J. Gan, College of Oceanic and Atmospheric Sciences, Oceanography Admin Building 104, Oregon State University, Corvallis, OR 07331–5503, USA. (jallen@coas.oregonstate.edu; gan@coas.oregonstate.edu)